Chapter 4

Collider signatures of the flavon of the $\mathscr{Z}_N \times \mathscr{Z}_M$ flavour symmetries

In the scenario, where the flavour scale Λ of $\mathscr{Z}_N \times \mathscr{Z}_M$ flavour symmetries is relatively low, closer to the weak scale, it would also be possible to investigate the direct production of flavons in hadron colliders, like the Large Hadron Collider (LHC). In this chapter, we now discuss the collider signatures of the flavon of the $\mathscr{Z}_N \times \mathscr{Z}_M$ flavour symmetries through its decays and production processes.

This chapter[1] will proceed along the following track : We first discuss the decays of flavon to a pair of fermions in section 4.1, as well as decays of top quark involving flavon in section 4.2. After this, in section 4.3, we investigate the production mechanisms of the flavon of the $\mathscr{Z}_N \times \mathscr{Z}_M$ flavour symmetries. Our aim is to identify different $\mathscr{Z}_N \times \mathscr{Z}_M$ flavour symmetries as much as possible through the collider signatures. Therefore, we shall finally discuss the sensitivity of signatures of different $\mathscr{Z}_N \times \mathscr{Z}_M$ flavour symmetries to the HL-LHC, the HE-LHC, and a 100 TeV collider. We classify the search for flavons into low and high-mass regions, with

[1]This chapter is based on the paper Phys.Rev.D 110 (2024) 11, 115015.

the low-mass region being particularly sensitive to the new symmetry-conserving mass mechanism of the pseudoscalar flavon.

For collider investigation, we also employ the parameter space of the flavon of the $\mathscr{Z}_N \times \mathscr{Z}_M$ flavour symmetries provided by the observable $R_{\mu\mu}$ in figure 3.7c. The observable $R_{\mu\mu}$ is sufficiently capable of differentiating the $\mathscr{Z}_N \times \mathscr{Z}_M$ flavour symmetries investigated in this work. For instance, we use the lower boundary of the allowed region of the parameter space corresponding to the $\mathscr{Z}_2 \times \mathscr{Z}_5$ flavour symmetry, which does not overlap with the parameter space corresponding to the $\mathscr{Z}_2 \times \mathscr{Z}_9$ flavour symmetry.

In the framework of $\mathscr{Z}_N \times \mathscr{Z}_M$ flavour symmetries, there is no Higgs-flavon mixing. Therefore, the flavon does not directly couple to the gauge bosons. This fact leads to no constraints on low masses of flavon from the direct LHC searches [194]. Moreover, the WW and ZZ decyas of flavon occur at one-loop level, and are much suppressed. The WW and ZZ final states searches set limits on masses above 300 GeV from ATLAS [195] and 200 GeV from CMS [196]. The searches in the di-photon channel place bounds on the masses above 200 GeV from the ATLAS [197], and above 500 GeV from the CMS [198].

4.1 Flavon decays to a pair of fermions

The flavon of the $\mathscr{Z}_N \times \mathscr{Z}_M$ flavour symmetries decays to a pair of fermions at tree-level, while the decays $a \to gg$ and $a \to \gamma\gamma$ are loop-induced. This is due to the non-zero off-diagonal couplings of the flavon to fermions. The partial decay width of the decay $a \to f_i \bar{f}_j$ at the tree-level can be written as,

$$\Gamma(a \to f_i \bar{f}_j) = \frac{N_c m_a}{16\pi} \left[\frac{(m_a^2 - (m_i + m_j)^2)(m_a^2 - (m_i - m_j)^2)}{m_a^4} \right]^{1/2} \left[\left(|y_{ij}|^2 + |y_{ji}|^2 \right) \left(1 - \frac{m_i^2 + m_j^2}{m_a^2} \right) - 2 \left(y_{ij} y_{ji} + y_{ij}^* y_{ji}^* \right) \frac{m_i m_j}{m_a^2} \right], \tag{4.1}$$

where N_c is the number of colors.

We present the branching ratios of $a \to f_i \bar{f}_j$, $a \to gg$ and $a \to \gamma\gamma$ in figure 4.1 for $\mathscr{Z}_2 \times \mathscr{Z}_{5,9,11}$ flavour symmetries , and in figure 4.2 for the $\mathscr{Z}_8 \times \mathscr{Z}_{22}$ flavour symmetry. In the quark sector, the dominant decay mode is $a \to b\bar{b}$ below the top quark threshold except for the minimal $\mathscr{Z}_2 \times \mathscr{Z}_5$ symmetry. For the minimal $\mathscr{Z}_2 \times \mathscr{Z}_5$ symmetry the mode $cu(c\bar{u}, \bar{c}u)$ prevails over other modes. This is due to the specific flavour structure of models based on the $\mathscr{Z}_N \times \mathscr{Z}_M$ flavour symmetries and the corresponding Yukawa couplings given in the appendix. As m_a approaches m_t, decay modes involving top quark, particularly, $tc(t\bar{c}, \bar{t}c)$, become increasingly significant for both the $\mathscr{Z}_2 \times \mathscr{Z}_{11}$ and $\mathscr{Z}_8 \times \mathscr{Z}_{22}$ models. These top quark related decay modes, however, remain comparatively less prominent than the decay modes of the flavon involving bottom and charm quark, such as, bd, bs, cc, cu, and bb for $\mathscr{Z}_2 \times \mathscr{Z}_5$ as well as $\mathscr{Z}_2 \times \mathscr{Z}_9$ symmetries, even beyond the top-threshold. Among the leptonic decay modes, the decay channels involving at least one τ dominate for all $\mathscr{Z}_N \times \mathscr{Z}_M$ flavour symmetries.

At $m_a > m_t$, in contrast to the other three $\mathscr{Z}_N \times \mathscr{Z}_M$ flavour symmetries, the $\mathscr{Z}_8 \times \mathscr{Z}_{22}$ model exhibits a dominant decay of the flavon into top quark pairs $(t\bar{t})$, as shown by the dashed-blue line in figure 4.2a. This striking feature arises from the construction of the $\mathscr{Z}_8 \times \mathscr{Z}_{22}$ model, where the top quark couples to the flavon with a suppression factor of order ε. Notably, this feature is absent in the remaining three $\mathscr{Z}_N \times \mathscr{Z}_M$ symmetry-based models under investigation. This feature keeps apart the

$\mathscr{Z}_8 \times \mathscr{Z}_{22}$ based model from the other models in terms of collider signatures, which are discussed in the later part of this work.

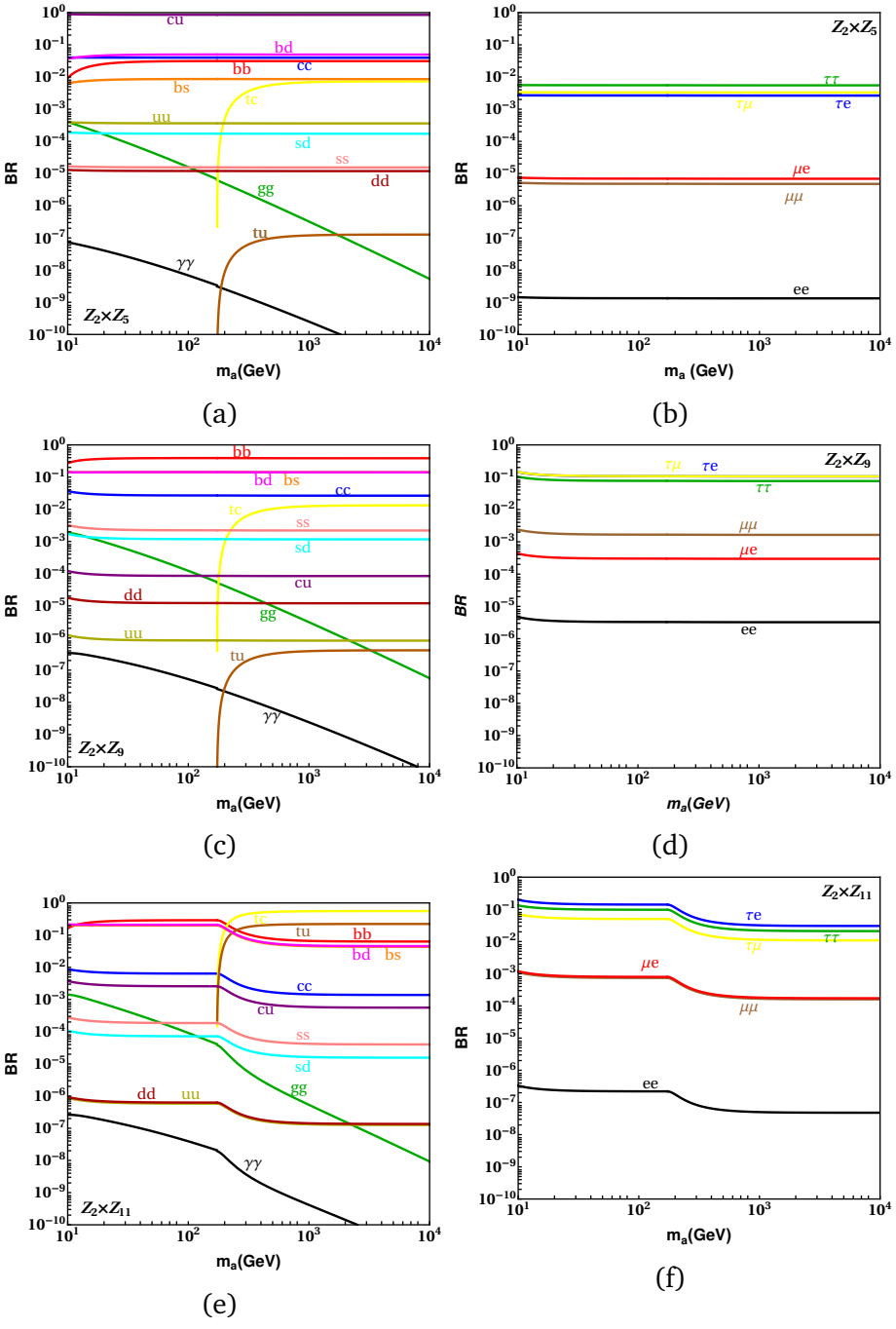

Fig. 4.1 Branching ratios of the various possible decay modes of the flavon into quark and lepton pairs for $\mathscr{Z}_2 \times \mathscr{Z}_5$, $\mathscr{Z}_2 \times \mathscr{Z}_9$, and $\mathscr{Z}_2 \times \mathscr{Z}_{11}$ flavour symmetries.

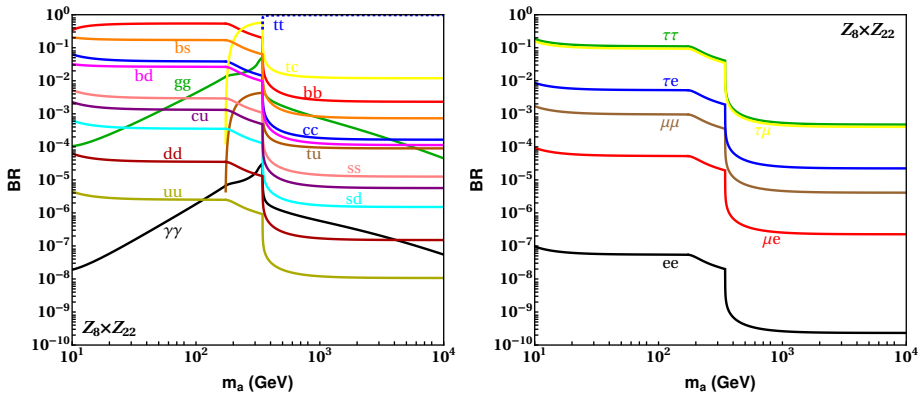

(a) (b)

Fig. 4.2 Branching ratios of the various possible decay modes of the flavon into quark and lepton pairs for $\mathscr{Z}_8 \times \mathscr{Z}_{22}$ flavour symmetry.

4.2 Top quark decays to flavon

The top quark decays to flavon play an important role in constraining a low-mass flavon. For the flavon mass, which is less than the mass of the top quark, anomalous top decays $t \to ac(au)$ provide distinguished signatures of flavon at hadron colliders. For Higgs production via such anomalous top-quark decays, the limits for the expected reach of the current 14 TeV LHC, HE-LHC, as well as a future high luminosity 100 TeV hadron collider are known, which can also be utilized for the flavon production. The current and expected limits on such processes at the LHC and a 100 TeV hadron collider are [103, 199],

$$\begin{aligned} BR_{8\ TeV}(t \to Hc) &< 5.6 \cdot 10^{-3}, \\ BR_{14\ TeV,3\ ab^{-1}}(t \to Hc) &< 4.5 \cdot 10^{-5}, \\ BR_{27\ TeV,15\ ab^{-1}}(t \to Hc) &< 9.7 \cdot 10^{-6}, \\ BR_{100\ TeV,30\ ab^{-1}}(t \to Hc) &< 2.2 \cdot 10^{-6}. \end{aligned} \tag{4.2}$$

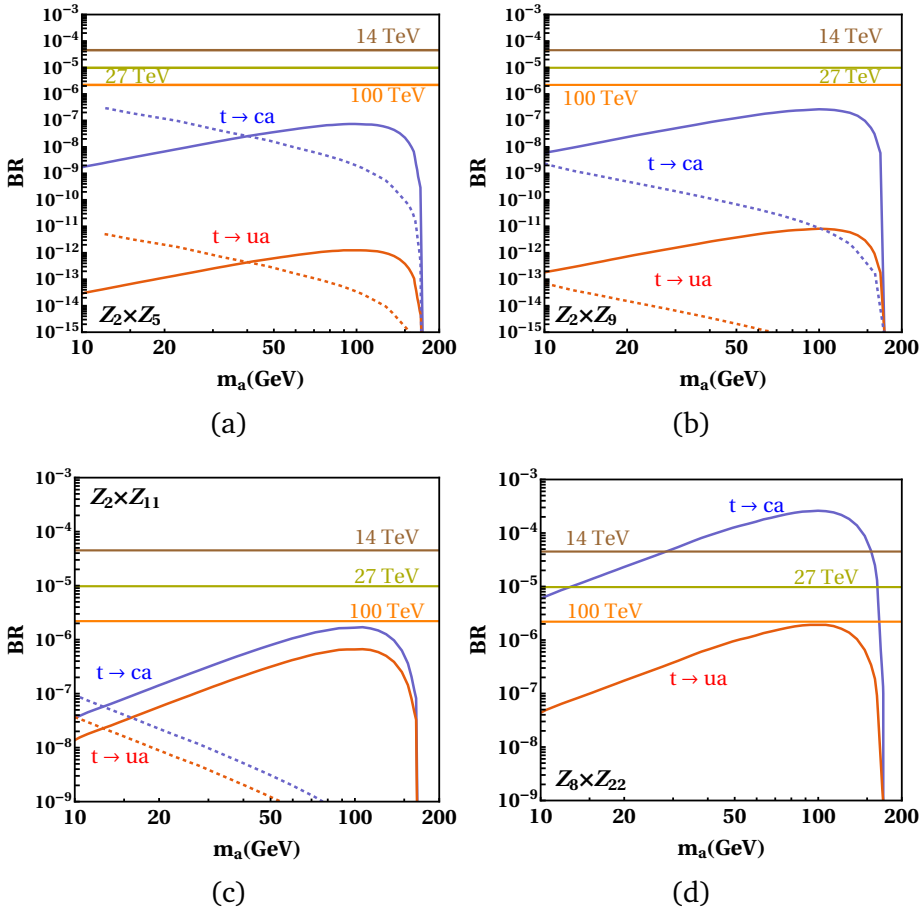

Fig. 4.3 The branching ratios of top quark decays into flavon of $\mathscr{Z}_N \times \mathscr{Z}_M$ flavour symmetries as a function of the flavon mass (m_a) along the parameter space allowed by the observable $R_{\mu\mu}$ in the phase-II of the LHCb for soft-symmetry breaking scenario, and $BR(K_L \to \mu^+\mu^-)$ for symmetry-conserving scenario.

In figure 4.3, we show the predictions of branching ratios for decays $t \to (c,u)a$ in the framework of different $\mathscr{Z}_N \times \mathscr{Z}_M$ flavour symmetries. We note that in the case of the soft symmetry-breaking scenario, shown by the solid continuous curves, the top decays to the flavon are investigated along the boundaries of parameter space allowed by the observable $R_{\mu\mu}$ in the phase-II of the LHCb, shown in figure 3.7c. With mass range m_a lying between 10 up to 200 GeV, the corresponding ranges for the VEV of the flavon f varies approximately as $\sim (2\times10^3, 4\times10^4)$ GeV for $\mathscr{Z}_2 \times \mathscr{Z}_5$, $\sim (10^3, 2\times10^4)$ GeV for $\mathscr{Z}_2 \times \mathscr{Z}_9$, $\sim (9\times10^3 - 1.4\times10^5)$ GeV for $\mathscr{Z}_2 \times \mathscr{Z}_{11}$,

and $\sim (4\times 10^2 - 10^4)$ GeV for $\mathscr{Z}_8 \times \mathscr{Z}_{22}$ flavour symmetry. We observe that only the flavon of the $\mathscr{Z}_8 \times \mathscr{Z}_{22}$ has the potential to reach the sensitivity of the 14 TeV LHC, the HE-LHC, and a 100 TeV future hadron collider. This prediction is very specific to test the $\mathscr{Z}_8 \times \mathscr{Z}_{22}$ flavour symmetry.

For the symmetry-conserving scenario, represented by the dashed curves in figure 4.3, we analyze $t \to (c,u)a$ decays along the parameter space allowed by the observable $BR(K_L \to \mu^+\mu^-)$, where VEV f ranges approximately as $\sim (3\times 10^3, 6\times 10^4)$ GeV for $\mathscr{Z}_2 \times \mathscr{Z}_5$, $\sim (4\times 10^4, 9\times 10^5)$ GeV for $\mathscr{Z}_2 \times \mathscr{Z}_9$, and $\sim (1.2\times 10^5, 2\times 10^6)$ GeV for $\mathscr{Z}_2 \times \mathscr{Z}_{11}$ flavour symmetry. It turns out that the decays $t \to ac(au)$ in the case of symmetry-conserving scenario for a light flavon are beyond the reach of the LHC, the HE-LHC, and a future 100 TeV hadron collider.

In figure 4.4, we show the prediction of branching ratios of decays $t \to (c,u)a$ for different $\mathscr{Z}_N \times \mathscr{Z}_M$ flavour symmetries for the flavon VEV $f = 500$ GeV in the soft symmetry-breaking case. This is a conventional choice in literature [103]. In this scenario, the branching ratio of the decay $t \to ca$ is accessible to a future 100 TeV hadron collider in a certain mass range for all $\mathscr{Z}_N \times \mathscr{Z}_M$ flavour symmetries discussed in this work. For the symmetries $\mathscr{Z}_2 \times \mathscr{Z}_{5,9}$, the branching ratio of the decay $t \to ca$ is of the order $10^{-6} - 10^{-5}$ for $m_a \leq 150$ GeV. The branching ratio of the decay $t \to ca$ is larger, and is maximally of the order of 10^{-3} for the $\mathscr{Z}_2 \times \mathscr{Z}_{11}$ and $\mathscr{Z}_8 \times \mathscr{Z}_{22}$ flavour symmetries.

The decay $t \to ca$ can be within the limits of the LHC, HE-LHC and a 100 TeV fulture hadron collider for the $\mathscr{Z}_2 \times \mathscr{Z}_{11}$ and $\mathscr{Z}_8 \times \mathscr{Z}_{22}$ flavour symmetries. This is a remarkable prediction of this work. The decay $t \to ca$ is within the reach of the limits of the HE-LHC for the $\mathscr{Z}_2 \times \mathscr{Z}_{5,9}$ flavour symmetries. We notice another important prediction of this work for the branching ratio of the decay $t \to ua$, which is in the reach of LHC, HE-LHC and a 100 TeV collider only for the $\mathscr{Z}_2 \times \mathscr{Z}_{11}$ flavour

symmetry. This decay is accessible to the HE-LHC only for the $\mathscr{Z}_8 \times \mathscr{Z}_{22}$ flavour symmetry. Thus, we conclude that the decays $t \to (c,u)a$ can be a good test ground for different $\mathscr{Z}_N \times \mathscr{Z}_M$ flavour symmetries for a low mass flavon.

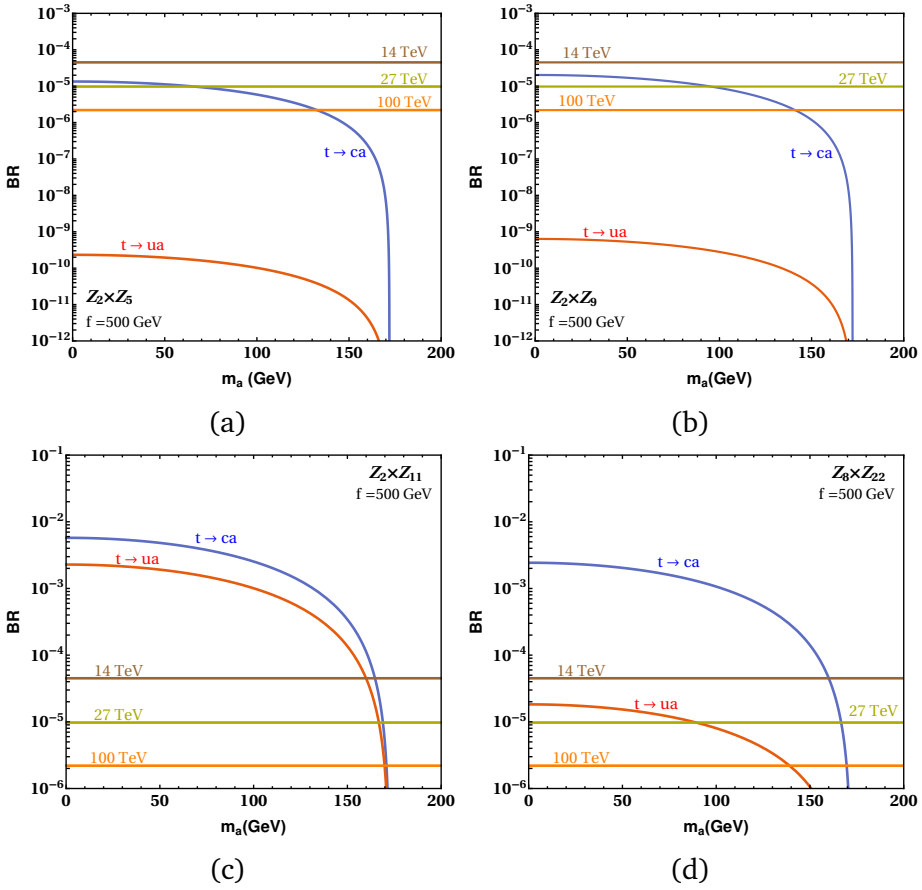

Fig. 4.4 Branching ratios of top quark decays into flavon of $\mathscr{Z}_2 \times \mathscr{Z}_5$, $\mathscr{Z}_2 \times \mathscr{Z}_9$, $\mathscr{Z}_2 \times \mathscr{Z}_{11}$ and $\mathscr{Z}_8 \times \mathscr{Z}_{22}$ flavour symmetries as a function of m_a, assuming the flavon VEV $f = 500$ GeV.

The limits in equation 4.2 can be used to place bounds on the parameter space of the flavon of the $\mathscr{Z}_N \times \mathscr{Z}_M$ flavour symmetries, as shown in figure 4.5. We must note that dashed straight lines denote our predictions for the symmetry-conserving scenarios, which are beyond the reach of the sensitivities given in equation 4.2.

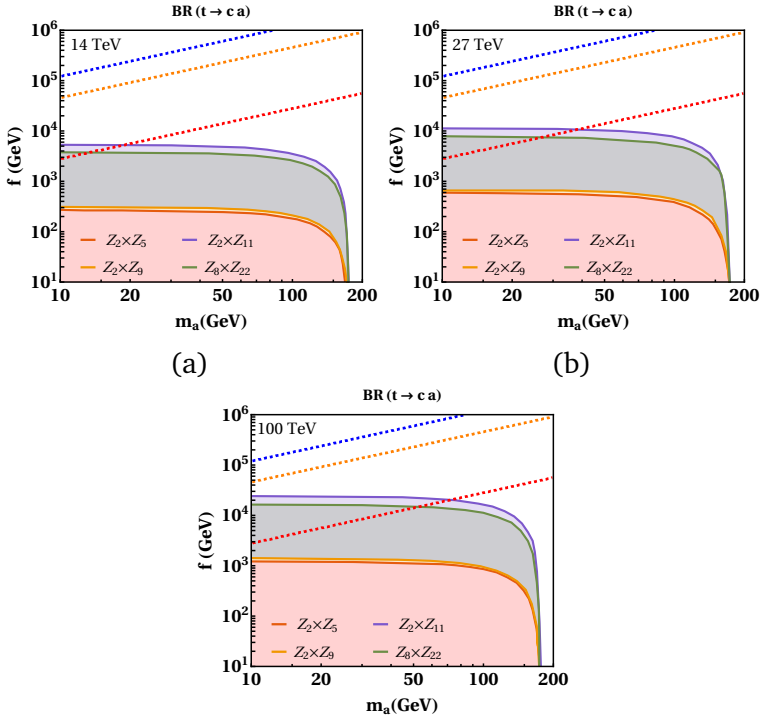

Fig. 4.5 The parameter space excluded by the limits on BR ($t \to Hc$) from 14 TeV LHC, 27 TeV HE-LHC, and a 100 TeV collider for $\mathscr{Z}_2 \times \mathscr{Z}_5$, $\mathscr{Z}_2 \times \mathscr{Z}_9$, $\mathscr{Z}_2 \times \mathscr{Z}_{11}$ and $\mathscr{Z}_8 \times \mathscr{Z}_{22}$ flavour symmetries in the soft symmetry-breaking scenario is shown with the coloured regions. The dashed lines represents the allowed parameter space in the symmetry-conserving scenario.

4.3 Flavon production at the HL-LHC, HE-LHC, and a 100 TeV hadron collider

We now discuss the production of the flavon of the $\mathscr{Z}_N \times \mathscr{Z}_M$ flavour symmetries at the LHC, HE-LHC, and at a 100 TeV future hadron collider. The analytical results for the production cross-sections of the flavon in various channels have been derived using the `MSTW2008` PDF [200]. Additionally, `FeynRules` [201] has been utilized to produce the model `UFO` files for all four $\mathscr{Z}_N \times \mathscr{Z}_M$ flavour symmetries discussed in

this work. We have used these files to perform production cross-section calculations with `MadGraph` [202], and verify our analytical results.

The inclusive production cross-sections of flavon of the $\mathscr{Z}_N \times \mathscr{Z}_M$ flavour symmetries at the LHC, HE-LHC, and at a 100 TeV future hadron collider are shown in figures 4.6 and 4.7 for the $\mathscr{Z}_2 \times \mathscr{Z}_{5,9,11}$ and the $\mathscr{Z}_8 \times \mathscr{Z}_{22}$ flavour symmetries. For the soft symmetry-breaking scenario, the boundaries of parameter space allowed by the observable $R_{\mu\mu}$ in the phase-II of the LHCb, shown in figure 3.7c, are used. The dashed curves are the cross-sections for the symmetry-conserving scenarios using the parameter space allowed by the observable $BR(K_L \to \mu^+\mu^-)$.

We use the parameter space allowed by the projected sensitivities of $\mathscr{R}_{\mu\mu}$ in the LHCb Phase-II in figure 3.7c to show the production cross-sections of a heavy flavon in the different $\mathscr{Z}_N \times \mathscr{Z}_M$ models. Furthermore, the most optimistic scenario is obtained using the flavon VEV $f = 500$ GeV, which is approximately allowed for a heavy flavon by the bounds obtained from the current measurement of the observable $R_{\mu\mu}$ in figure 3.7a. This choice is also used in previous works, such as references [97, 103]. We continue to use the flavon VEV $f = 500$ GeV even for the production cross-sections of a low mass flavon.

In the soft symmetry-breaking scenario, the projected sensitivities of $\mathscr{R}_{\mu\mu}$ in the LHCb Phase-II allows the mass range m_a lying between 10 up to 10^4 GeV, the corresponding ranges for the VEV of the flavon f vary approximately as $\sim (3\times10^2, 4\times10^4)$ GeV for $\mathscr{Z}_2 \times \mathscr{Z}_5$, $\sim (6\times10^2, 2.6\times10^4)$ GeV for $\mathscr{Z}_2 \times \mathscr{Z}_9$, $\sim (7.8\times 10^2, 1.4\times10^5)$ GeV for $\mathscr{Z}_2 \times \mathscr{Z}_{11}$, and $\sim (3.6\times10^2, 10^4)$ GeV for $\mathscr{Z}_8 \times \mathscr{Z}_{22}$ flavour symmetry.

For the symmetry-conserving scenario, we analyze flavon production channels with the parameter space allowed the observable $\mathrm{BR}(K_L \to \mu^+\mu^-)$, where VEV f

ranges approximately as $\sim (3\times10^3, 3\times10^6)$ GeV for $\mathscr{Z}_2\times\mathscr{Z}_5$, $\sim (4\times10^4, 4\times10^7)$ GeV for $\mathscr{Z}_2\times\mathscr{Z}_9$, and $\sim (10^5, 9\times10^7)$ GeV for $\mathscr{Z}_2\times\mathscr{Z}_{11}$ flavour symmetry.

4.3.1 Inclusive production

A flavon can be produced through the inclusive channels,

$$gg, bb \to a. \tag{4.3}$$

As it can be noted from figure 4.6 and 4.7, the gluon-fusion production cross-sections for the soft symmetry-breaking scenario, is very small for the $\mathscr{Z}_2\times\mathscr{Z}_{5,9,11}$ flavour symmetries due to the absence of the flavour-diagonal coupling of the flavon to top quarks. However, this observation dramatically changes for the $\mathscr{Z}_8\times\mathscr{Z}_{22}$ flavour symmetry, where the flavour-diagonal coupling of the flavon to top quarks is allowed. This can be seen in figures 4.7d-4.7f. In the case of symmetry-conserving scenario, the gluon-fusion production cross-section turns out to be very small and, as will be shown later, is beyond the reach of the LHC, HE-LHC, and a 100 TeV future collider.

In figures 4.8 and 4.9, we show the production cross-sections of the flavon of different $\mathscr{Z}_N\times\mathscr{Z}_M$ flavour symmetries for the VEV $f = 500$ GeV for the soft symmetry-breaking scenario. In this scenario, the production cross-sections can be sufficiently large for the $\mathscr{Z}_2\times\mathscr{Z}_{5,9,11}$ and $\mathscr{Z}_8\times\mathscr{Z}_{22}$ flavour symmetries. Therefore, our investigation of the inclusive modes will be performed only for this choice from now on for the heavy mass flavon.

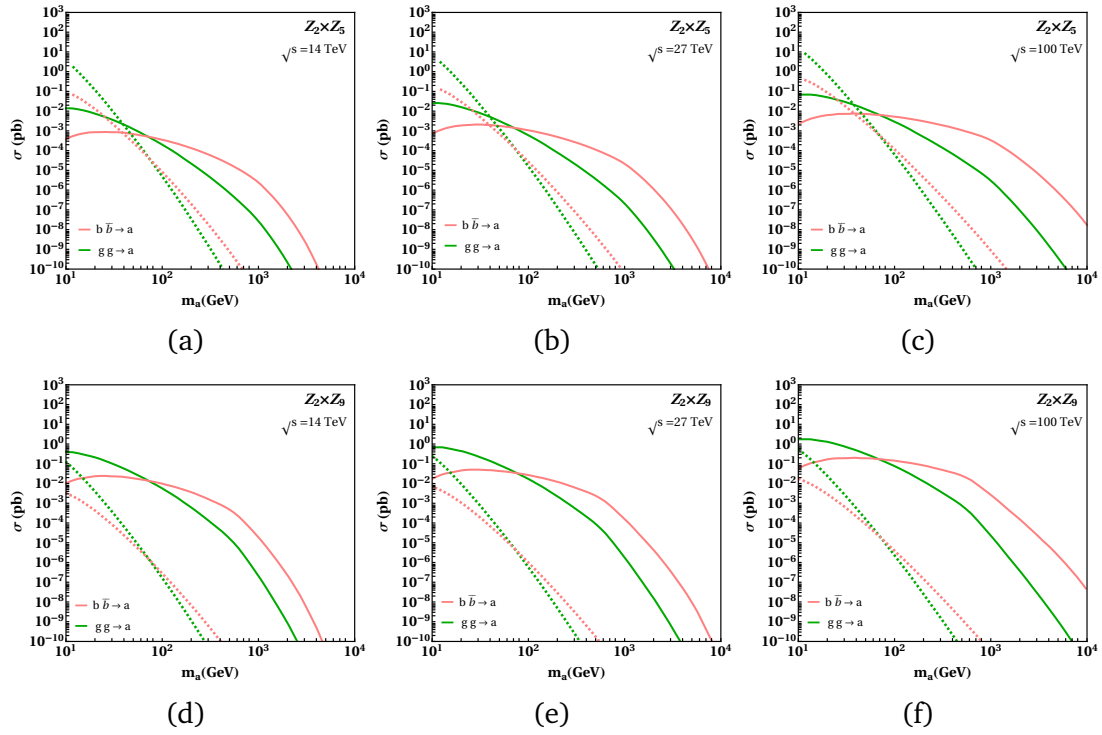

Fig. 4.6 Production cross-sections of the flavon of $\mathscr{Z}_2 \times \mathscr{Z}_5$, $\mathscr{Z}_2 \times \mathscr{Z}_9$ flavour symmetries with respect to its mass through different channels for the 14 TeV HL-LHC, 27 TeV HE-LHC, and future 100 TeV hadron collider. The solid lines represents the production cross section along the boundaries of parameter space allowed by the observable $R_{\mu\mu}$ for soft symmetry-breaking scenario, while the dashed lines correspond to that in the symmetry-conserving scenario along the allowed parameter space by the observable $BR(K_L \to \mu\mu)_{SD}$.

The above results can be used to look for resonance searches of the flavon. For example, a generic search is of the type,

$$pp \to a \to b\bar{b}/\ell_i\ell_i/\gamma\gamma\,. \tag{4.4}$$

On the other side, due to the off-diagonal flavon couplings of flavon to a fermionic pair, searches with a specific signature of the $\mathscr{Z}_{\rm N} \times \mathscr{Z}_{\rm M}$ flavour symmetries are,

$$pp \to a \to t\bar{c}/t\bar{u}. \tag{4.5}$$

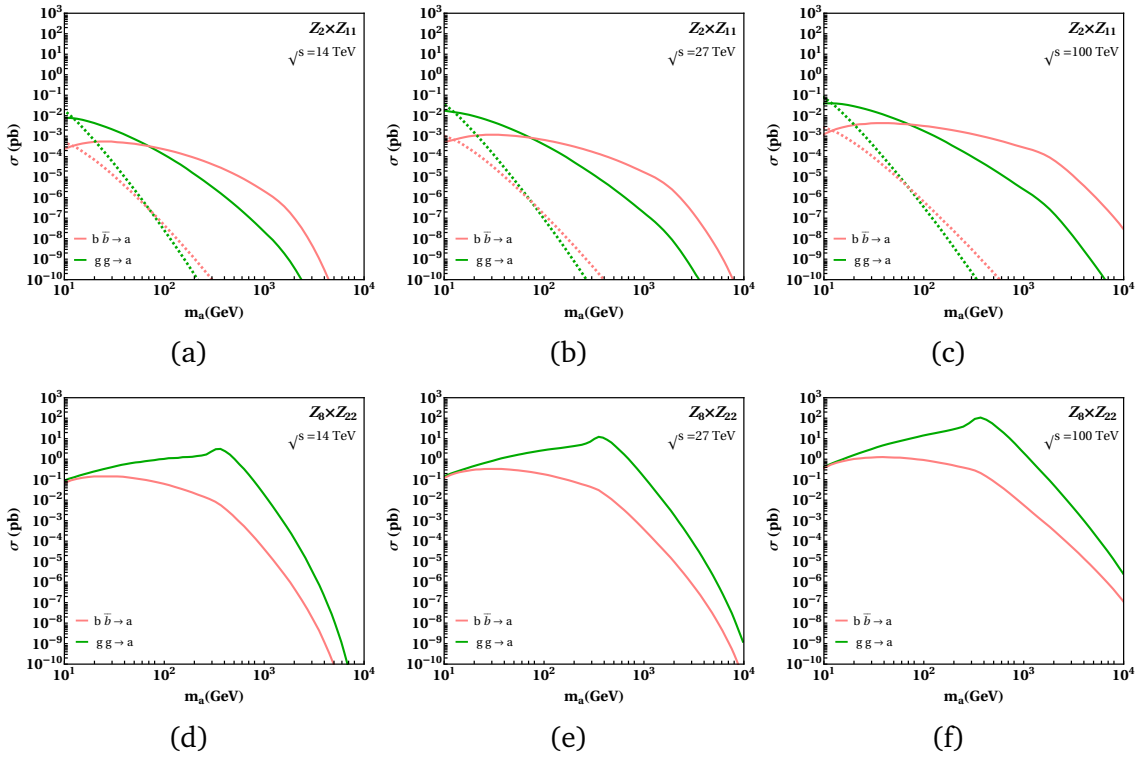

Fig. 4.7 Production cross-sections of the flavon of $\mathscr{Z}_2 \times \mathscr{Z}_{11}$, and $\mathscr{Z}_8 \times \mathscr{Z}_{22}$ flavour symmetries with respect to its mass through different channels for the 14 TeV HL-LHC, 27 TeV HE-LHC, and future 100 TeV hadron collider. The solid lines represents the production cross section along the boundaries of parameter space allowed by the observable $R_{\mu\mu}$ for soft symmetry-breaking scenario, while the dashed lines correspond to that in the symmetry-conserving scenario along the allowed parameter space by the observable $BR(K_L \to \mu\mu)_{SD}$.

In table 4.1, we show the present sensitivities of different inclusive flavon production channels at the 14 TeV LHC. These results will be used to estimate the sensitivities of the HL-LHC, HE-LHC, and a 100 TeV collider for a heavy flavon production and decay. We show these sensitivities in table 4.2. These sensitivities are estimated using simple square root scaling of the luminosity of the LHC by,

$$\mathscr{S} \simeq \frac{S}{\sqrt{B}} \simeq \sqrt{\mathscr{L}} \frac{\sigma_s}{\sqrt{\sigma_B}}, \tag{4.6}$$

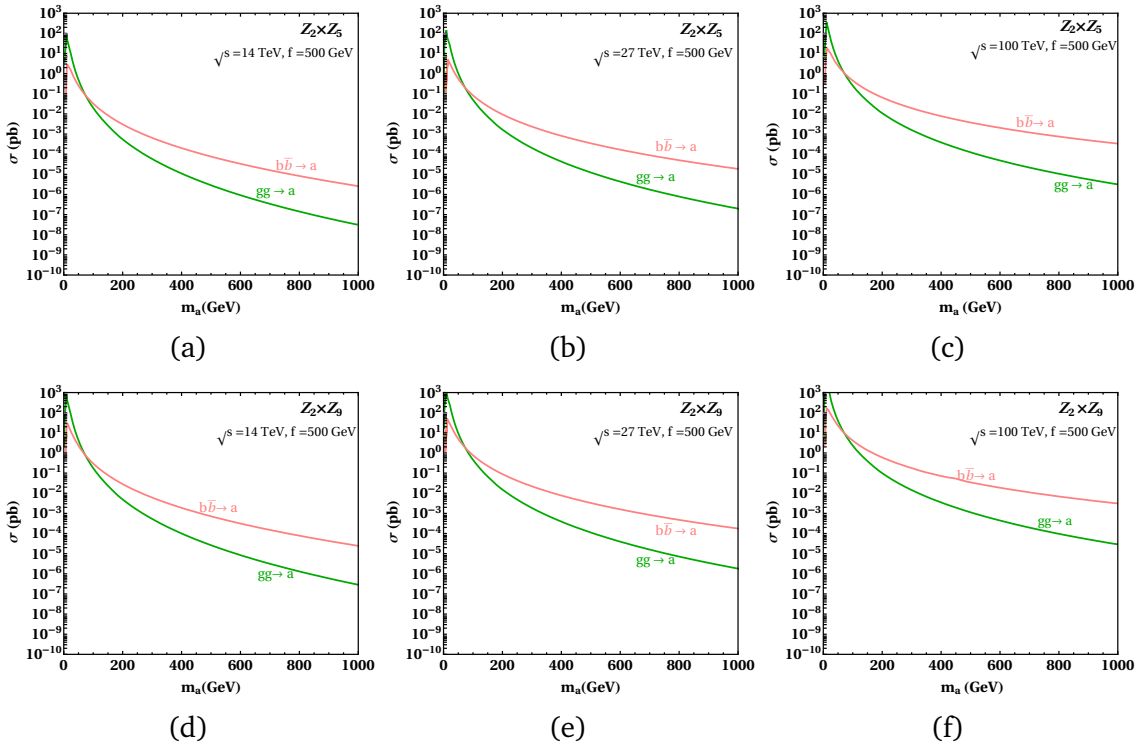

Fig. 4.8 Production cross-sections of the flavon of $\mathscr{Z}_2 \times \mathscr{Z}_5$, and $\mathscr{Z}_2 \times \mathscr{Z}_9$ flavour symmetries with respect to its mass through different channels for 14 TeV HL-LHC, 27 TeV HE-LHC, and future 100 TeV hadron collider, where the flavon VEV $f = 500$ GeV.

	$\mathscr{L}[fb^{-1}]$ [References]		ATLAS 13 TeV		CMS 13 TeV	
m_a [GeV]	ATLAS	CMS	500	1000	500	1000
jet-jet [pb]	139 [203]	137 [204]		0.1		0.2
$\tau\tau$ [pb]	36.1 [205]	35.9 [206]	$8 \cdot 10^{-2}$	10^{-2}	$6 \cdot 10^{-2}$	10^{-2}
ee, $\mu\mu$ [pb]	139 [207]	140 [208]	$8 \cdot 10^{-4}$	$2 \cdot 10^{-4}$	$2 \cdot 10^{-3}$	$4 \cdot 10^{-4}$
μe [pb]	138 [209]	139 [210]		$3 \cdot 10^{-4}$	$4 \cdot 10^{-3}$	$3 \cdot 10^{-4}$
$\mu\tau$ [pb]	138 [209]	139 [210]		$1 \cdot 10^{-3}$	$7 \cdot 10^{-3}$	$1 \cdot 10^{-3}$
$e\tau$ [pb]	138 [209]	139 [210]		$1 \cdot 10^{-3}$	$5 \cdot 10^{-3}$	$1 \cdot 10^{-3}$
$b\bar{b}$ [pb]	139 [203]	138 [211]		$1 \cdot 10^{-2}$		$4 \cdot 10^{-2}$
$\gamma\gamma$ [pb]	139 [197]	35.9 [198]	$5 \cdot 10^{-4}$	$1 \cdot 10^{-4}$	$4 \cdot 10^{-3}$	$8 \cdot 10^{-4}$
$t\bar{t}$ [pb]	36.1 [212, 213]	35.9 [214]	$2 \cdot 10^{2}$	2	30	0.4

Table 4.1 Current limits for production cross section times branching ratio ($\sigma \times BR$) at 13 TeV LHC by ATLAS and CMS in high mass resonance searches for inclusive flavon production channels.

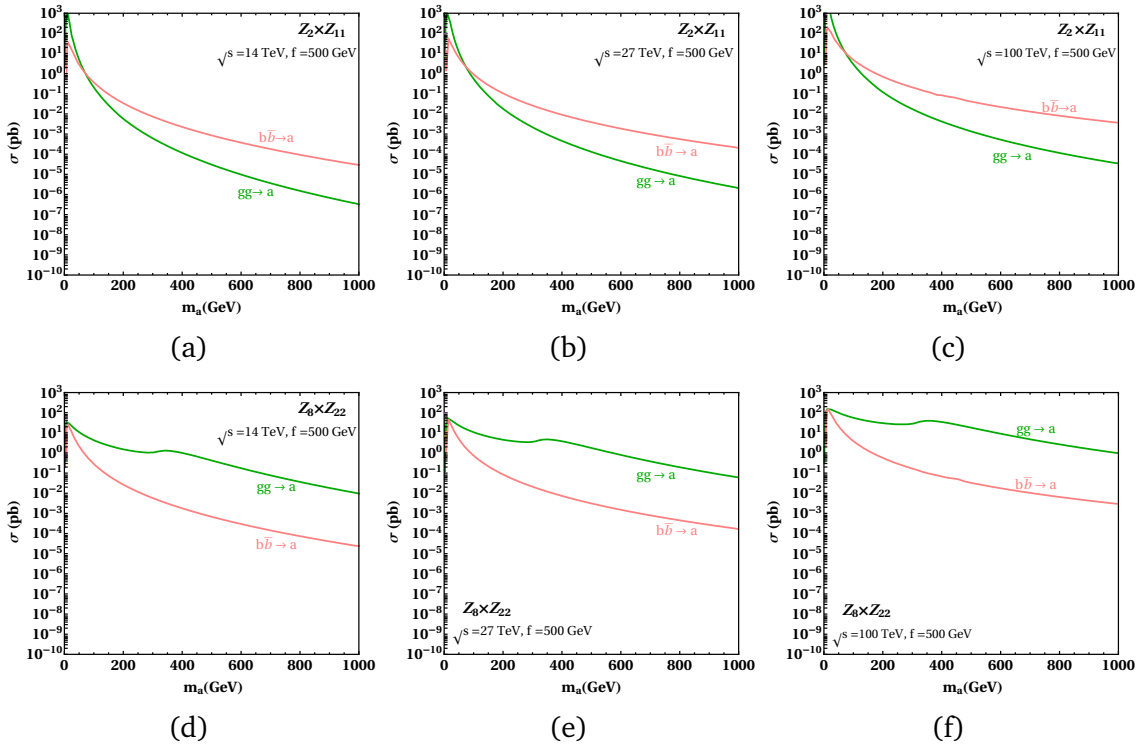

Fig. 4.9 Production cross-sections of the flavon of $\mathscr{Z}_2 \times \mathscr{Z}_{11}$, and $\mathscr{Z}_8 \times \mathscr{Z}_{22}$ flavour symmetries with respect to its mass through different channels for 14 TeV HL-LHC, 27 TeV HE-LHC, and future 100 TeV high-luminosity hadron collider, where the flavon VEV $f = 500$ GeV.

where S is the number of signal events, B denotes the background events, σ_s is the signal cross-section, and σ_B stands for the background cross-section.

We adopt a conservative approach for estimating the sensitivities of the HL-LHC, HE-LHC, and a 100 TeV collider. We make the following assumptions for this purpose.

1. The significance $\mathscr{S} \simeq \frac{S}{\sqrt{B}}$ remains constant among the colliders.

2. We assume that there is no appreciable change in the reconstruction efficiencies and background rejection.

We note that similar assumptions are also used in the “Collider Reach" tool, which remarkably provides an estimate of the mass of a BSM physics that can be searched at the LHC and a future collider [215].

Thus, the required sensitive cross-section of any flavon signal at a future collider (FC) is given by

$$\sigma_s^{\rm FC} = \sqrt{\frac{\mathscr{L}_{\rm LHC}}{\mathscr{L}_{\rm FC}}}\sqrt{\frac{\sigma_B^{FC}}{\sigma_B^{LHC}}}\sigma_s^{\rm LHC}, \tag{4.7}$$

where FC= HL-LHC, HE-LHC, and a 100 TeV collider. We have computed σ_B^{FC} and σ_B^{LHC} through MadGraph, and it turns out that $\sigma_B^{HE-LHC} \leq 2\sigma_B^{LHC}$ and $\sigma_B^{100TeV} \leq 10\sigma_B^{LHC}$, and σ_s^{LHC} is given in table 4.1.

	HL-LHC [14 TeV, 3 ab^{-1}]		HE-LHC [27 TeV, 15 ab^{-1}]		100 TeV, 30 ab^{-1}	
m_a [GeV]	500	1000	500	1000	500	1000
jet-jet [pb]		$4\cdot10^{-2}$		$3\cdot10^{-2}$		$4\cdot10^{-2}$
$\tau\tau$ [pb]	$7\cdot10^{-3}$	$1\cdot10^{-3}$	$4\cdot10^{-3}$	$7\cdot10^{-4}$	$5\cdot10^{-3}$	$8\cdot10^{-4}$
ee, $\mu\mu$ [pb]	$2\cdot10^{-4}$	$4\cdot10^{-5}$	$1\cdot10^{-4}$	$3\cdot10^{-5}$	$1\cdot10^{-4}$	$3\cdot10^{-5}$
μe [pb]	$9\cdot10^{-4}$	$7\cdot10^{-5}$	$7\cdot10^{-4}$	$5\cdot10^{-5}$	$1\cdot10^{-3}$	$1\cdot10^{-4}$
$\mu\tau$ [pb]	$2\cdot10^{-3}$	$2\cdot10^{-4}$	$1\cdot10^{-3}$	$2\cdot10^{-4}$	$2\cdot10^{-3}$	$3\cdot10^{-4}$
$e\tau$ [pb]	$1\cdot10^{-3}$	$2\cdot10^{-4}$	$8\cdot10^{-4}$	$2\cdot10^{-4}$	$1\cdot10^{-3}$	$3\cdot10^{-4}$
$b\bar{b}$ [pb]		$9\cdot10^{-3}$		$5\cdot10^{-3}$		$7\cdot10^{-3}$
$\gamma\gamma$ [pb]	$1\cdot10^{-4}$	$2\cdot10^{-5}$	$6\cdot10^{-5}$	$1\cdot10^{-5}$	$7\cdot10^{-5}$	$1\cdot10^{-5}$
$t\bar{t}$ [pb]	4	$5\cdot10^{-2}$	3	$4\cdot10^{-2}$	8	0.1

Table 4.2 Estimated reach ($\sigma \times BR$) of the HL-LHC, HE-LHC and a 100 TeV hadron collider for high flavon mass (m_a) in inclusive flavon production channels.

We show our benchmark predictions for the processes given in table 4.1, for different $\mathscr{Z}_{\rm N} \times \mathscr{Z}_{\rm M}$ flavour symmetries in tables 4.3- 4.5 for $f = 500$ GeV and $m_a = 500, 1000$ for the soft symmetry-breaking scenarios. The modes that are accessible to the HL-LHC, HE-LHC, and a 100 TeV collider are marked with a box $\square$.

From table 4.3, we observe that only the $\mathscr{Z}_2 \times \mathscr{Z}_5$ and the $\mathscr{Z}_8 \times \mathscr{Z}_{22}$ flavour symmetries are accessible to the HL-LHC, and both the symmetries can be differen-

tiated due to the distinct accessible processes. This situation changes sufficiently for the HE-LHC as shown in table 4.4, as more processes are under the reach of the HE-LHC. However, even now, mainly the $\mathscr{Z}_2 \times \mathscr{Z}_5$ and the $\mathscr{Z}_8 \times \mathscr{Z}_{22}$ flavour symmetries are under the reach of the HE-LHC. The $\mathscr{Z}_2 \times \mathscr{Z}_9$ flavour symmetry can be probed through the $e\tau$ channel.

	Benchmark $\mathscr{Z}_2 \times \mathscr{Z}_5$		Benchmark $\mathscr{Z}_2 \times \mathscr{Z}_9$		Benchmark $\mathscr{Z}_2 \times \mathscr{Z}_{11}$		Benchmark $\mathscr{Z}_8 \times \mathscr{Z}_{22}$	
m_a [GeV]	500	1000	500	1000	500	1000	500	1000
jet-jet [pb]		$\boxed{3.6 \cdot 10^{-2}}$		$1.5 \cdot 10^{-6}$		$2.3 \cdot 10^{-7}$		$1.4 \cdot 10^{-3}$
$\tau\tau$ [pb]	$1.2 \cdot 10^{-3}$	$9.2 \cdot 10^{-5}$	$8.0 \cdot 10^{-5}$	$3.4 \cdot 10^{-6}$	$2.9 \cdot 10^{-5}$	$1.6 \cdot 10^{-6}$	$3.4 \cdot 10^{-3}$	$6.1 \cdot 10^{-5}$
$\mu\tau$ [pb]	$1.4 \cdot 10^{-3}$	$1.1 \cdot 10^{-4}$	$2.3 \cdot 10^{-4}$	$9.5 \cdot 10^{-6}$	$3 \cdot 10^{-5}$	$1.7 \cdot 10^{-6}$	$\boxed{5.8 \cdot 10^{-3}}$	$1 \cdot 10^{-4}$
$e\tau$ [pb]	$\boxed{1.1 \cdot 10^{-3}}$	$8.9 \cdot 10^{-5}$	$2.2 \cdot 10^{-4}$	$9.4 \cdot 10^{-6}$	$8.5 \cdot 10^{-5}$	$4.7 \cdot 10^{-6}$	$3.2 \cdot 10^{-4}$	$5.8 \cdot 10^{-6}$
$\mu\mu$ [pb]	$1.1 \cdot 10^{-6}$	$8.3 \cdot 10^{-8}$	$1.7 \cdot 10^{-6}$	$7.3 \cdot 10^{-8}$	$2.2 \cdot 10^{-7}$	$1.2 \cdot 10^{-8}$	$2.9 \cdot 10^{-5}$	$5.3 \cdot 10^{-7}$
μe [pb]	$2.9 \cdot 10^{-6}$	$2.3 \cdot 10^{-7}$	$6.3 \cdot 10^{-7}$	$2.6 \cdot 10^{-8}$	$4.8 \cdot 10^{-7}$	$2.7 \cdot 10^{-8}$	$3.3 \cdot 10^{-6}$	$5.8 \cdot 10^{-8}$
ee [pb]	$2.5 \cdot 10^{-10}$	$2 \cdot 10^{-11}$	$3.4 \cdot 10^{-9}$	$1.4 \cdot 10^{-10}$	$6.7 \cdot 10^{-11}$	$3.7 \cdot 10^{-12}$	$1.7 \cdot 10^{-9}$	$3 \cdot 10^{-11}$
$\gamma\gamma$ [pb]	$1.3 \cdot 10^{-7}$	$3.6 \cdot 10^{-9}$	$8.2 \cdot 10^{-10}$	$1.2 \cdot 10^{-11}$	$1.5 \cdot 10^{-10}$	$3 \cdot 10^{-12}$	$\boxed{6.6 \cdot 10^{-4}}$	$1 \cdot 10^{-5}$
$b\bar{b}$ [pb]	$9.8 \cdot 10^{-3}$	$6.3 \cdot 10^{-4}$	$4.7 \cdot 10^{-4}$	$1.9 \cdot 10^{-5}$	$1.2 \cdot 10^{-4}$	$5.7 \cdot 10^{-6}$	$1.9 \cdot 10^{-2}$	$3.2 \cdot 10^{-4}$
tc [pb]	$3.6 \cdot 10^{-3}$	$2.8 \cdot 10^{-4}$	$2.5 \cdot 10^{-5}$	$1.2 \cdot 10^{-6}$	$1.5 \cdot 10^{-3}$	$8.5 \cdot 10^{-5}$	0.152	$3.1 \cdot 10^{-3}$
tu [pb]	$6.5 \cdot 10^{-8}$	$5.1 \cdot 10^{-9}$	$7.8 \cdot 10^{-10}$	$3.8 \cdot 10^{-11}$	$6.6 \cdot 10^{-4}$	$3.8 \cdot 10^{-5}$	$1.1 \cdot 10^{-3}$	$2.3 \cdot 10^{-5}$
$t\bar{t}$ [pb]							$\boxed{4.42}$	0.12

Table 4.3 Benchmark points for different $\mathscr{Z}_N \times \mathscr{Z}_M$ flavour symmetries for inclusive flavon production channels with high flavon mass (m_a) in case of the soft symmetry-breaking scenario at the 14 TeV HL-LHC, assuming VEV (f) $= 500$ GeV. Accessible channels are represented within the box.

A 100 TeV collider provides a more dramatic scenario for the $\mathscr{Z}_\mathrm{N} \times \mathscr{Z}_\mathrm{M}$ flavour symmetries. As shown in table 4.5, all symmetries except the $\mathscr{Z}_2 \times \mathscr{Z}_{11}$ become sensitive in most of the inclusive processes. The $\mathscr{Z}_2 \times \mathscr{Z}_{11}$ flavour symmetry is accessible only through the $e\tau$ channel.

	Benchmark $\mathscr{Z}_2 \times \mathscr{Z}_5$		Benchmark $\mathscr{Z}_2 \times \mathscr{Z}_9$		Benchmark $\mathscr{Z}_2 \times \mathscr{Z}_{11}$		Benchmark $\mathscr{Z}_8 \times \mathscr{Z}_{22}$	
m_a [GeV]	500	1000	500	1000	500	1000	500	1000
jet-jet [pb]		0.133		$8.2 \cdot 10^{-6}$		$9.4 \cdot 10^{-7}$		$9.8 \cdot 10^{-3}$
$\tau\tau$ [pb]	$2.6 \cdot 10^{-3}$	$2.8 \cdot 10^{-4}$	$2.9 \cdot 10^{-4}$	$1.7 \cdot 10^{-5}$	$8 \cdot 10^{-5}$	$5.6 \cdot 10^{-6}$	$1.5 \cdot 10^{-2}$	$4 \cdot 10^{-4}$
$\mu\tau$ [pb]	$3.2 \cdot 10^{-3}$	$3.5 \cdot 10^{-4}$	$8.3 \cdot 10^{-4}$	$4.8 \cdot 10^{-5}$	$8.4 \cdot 10^{-5}$	$5.8 \cdot 10^{-6}$	$2.5 \cdot 10^{-2}$	$6.8 \cdot 10^{-4}$
$e\tau$ [pb]	$2.6 \cdot 10^{-3}$	$2.8 \cdot 10^{-4}$	$8.2 \cdot 10^{-4}$	$4.8 \cdot 10^{-5}$	$2.3 \cdot 10^{-4}$	$1.6 \cdot 10^{-5}$	$1.4 \cdot 10^{-3}$	$3.8 \cdot 10^{-5}$
$\mu\mu$ [pb]	$2.4 \cdot 10^{-6}$	$2.6 \cdot 10^{-7}$	$6.4 \cdot 10^{-6}$	$3.7 \cdot 10^{-7}$	$6.2 \cdot 10^{-7}$	$4.3 \cdot 10^{-8}$	$1.3 \cdot 10^{-4}$	$3.5 \cdot 10^{-6}$
μe [pb]	$6.6 \cdot 10^{-6}$	$7.1 \cdot 10^{-7}$	$2.3 \cdot 10^{-6}$	$1.4 \cdot 10^{-7}$	$1.3 \cdot 10^{-6}$	$9.3 \cdot 10^{-8}$	$1.4 \cdot 10^{-5}$	$3.8 \cdot 10^{-7}$
ee [pb]	$5.6 \cdot 10^{-10}$	$6.1 \cdot 10^{-11}$	$1.3 \cdot 10^{-8}$	$7.4 \cdot 10^{-10}$	$1.8 \cdot 10^{-10}$	$1.3 \cdot 10^{-11}$	$7.2 \cdot 10^{-9}$	$1.9 \cdot 10^{-10}$
$\gamma\gamma$ [pb]	$2.9 \cdot 10^{-7}$	$1.1 \cdot 10^{-8}$	$3 \cdot 10^{-9}$	$6.3 \cdot 10^{-11}$	$4.2 \cdot 10^{-10}$	$1.1 \cdot 10^{-11}$	$2.8 \cdot 10^{-3}$	$6.7 \cdot 10^{-5}$
$b\bar{b}$ [pb]	$2.7 \cdot 10^{-2}$	$2.3 \cdot 10^{-3}$	$1.9 \cdot 10^{-3}$	$1 \cdot 10^{-4}$	$3.8 \cdot 10^{-4}$	$2.3 \cdot 10^{-5}$	$8.8 \cdot 10^{-2}$	$2.2 \cdot 10^{-3}$
tc [pb]	$1 \cdot 10^{-2}$	$1 \cdot 10^{-3}$	$1 \cdot 10^{-4}$	$6.6 \cdot 10^{-6}$	$4.6 \cdot 10^{-3}$	$3.4 \cdot 10^{-4}$	0.702	$2.1 \cdot 10^{-2}$
tu [pb]	$1.8 \cdot 10^{-7}$	$1.9 \cdot 10^{-8}$	$3.1 \cdot 10^{-9}$	$2 \cdot 10^{-10}$	$2 \cdot 10^{-3}$	$1.5 \cdot 10^{-4}$	$5.3 \cdot 10^{-3}$	$1.6 \cdot 10^{-4}$
$t\bar{t}$ [pb]							20.46	0.83

Table 4.4 Benchmark points for different $\mathscr{Z}_N \times \mathscr{Z}_M$ flavour symmetries for inclusive flavon production channels with high flavon mass (m_a) in case of the soft symmetry-breaking scenario at the 27 TeV HE-LHC , assuming $f = 500$ GeV.

	Benchmark $\mathscr{Z}_2 \times \mathscr{Z}_5$		Benchmark $\mathscr{Z}_2 \times \mathscr{Z}_9$		Benchmark $\mathscr{Z}_2 \times \mathscr{Z}_{11}$		Benchmark $\mathscr{Z}_8 \times \mathscr{Z}_{22}$	
m_a [GeV]	500	1000	500	1000	500	1000	500	1000
jet-jet [pb]		0.95		$1.1 \cdot 10^{-4}$		$8.1 \cdot 10^{-6}$		0.18
$\tau\tau$ [pb]	$1.1 \cdot 10^{-2}$	$1.4 \cdot 10^{-3}$	$2.2 \cdot 10^{-3}$	$1.9 \cdot 10^{-4}$	$4.8 \cdot 10^{-4}$	$3.8 \cdot 10^{-5}$	0.14	$6.2 \cdot 10^{-3}$
$\mu\tau$ [pb]	$1.3 \cdot 10^{-2}$	$1.7 \cdot 10^{-3}$	$6.3 \cdot 10^{-3}$	$5.5 \cdot 10^{-4}$	$5 \cdot 10^{-4}$	$3.9 \cdot 10^{-5}$	0.23	$1.0 \cdot 10^{-2}$
$e\tau$ [pb]	$1.1 \cdot 10^{-2}$	$1.4 \cdot 10^{-3}$	$6.2 \cdot 10^{-3}$	$5.4 \cdot 10^{-4}$	$1.3 \cdot 10^{-3}$	$1.1 \cdot 10^{-4}$	$1.3 \cdot 10^{-2}$	$5.9 \cdot 10^{-4}$
$\mu\mu$ [pb]	$9.9 \cdot 10^{-5}$	$1.3 \cdot 10^{-6}$	$4.8 \cdot 10^{-5}$	$4.2 \cdot 10^{-6}$	$3.7 \cdot 10^{-6}$	$2.9 \cdot 10^{-7}$	$1.2 \cdot 10^{-3}$	$5.4 \cdot 10^{-5}$
μe [pb]	$2.8 \cdot 10^{-5}$	$3.5 \cdot 10^{-6}$	$1.7 \cdot 10^{-5}$	$1.5 \cdot 10^{-6}$	$8 \cdot 10^{-6}$	$6.3 \cdot 10^{-7}$	$1.3 \cdot 10^{-4}$	$5.9 \cdot 10^{-6}$
ee [pb]	$2.4 \cdot 10^{-9}$	$3.0 \cdot 10^{-10}$	$9.6 \cdot 10^{-8}$	$8.4 \cdot 10^{-9}$	$1.1 \cdot 10^{-9}$	$8.8 \cdot 10^{-11}$	$6.9 \cdot 10^{-8}$	$3.0 \cdot 10^{-9}$
$\gamma\gamma$ [pb]	$1.2 \cdot 10^{-6}$	$5.6 \cdot 10^{-8}$	$2.3 \cdot 10^{-8}$	$7.2 \cdot 10^{-10}$	$2.5 \cdot 10^{-9}$	$7.2 \cdot 10^{-11}$	$2.7 \cdot 10^{-2}$	$1 \cdot 10^{-3}$
$b\bar{b}$ [pb]	0.15	$1.7 \cdot 10^{-2}$	$1.7 \cdot 10^{-2}$	$1.3 \cdot 10^{-3}$	$2.7 \cdot 10^{-3}$	$2 \cdot 10^{-4}$	1.03	$4.1 \cdot 10^{-2}$
tc [pb]	$5.4 \cdot 10^{-2}$	$7.6 \cdot 10^{-3}$	$9.2 \cdot 10^{-4}$	$8.9 \cdot 10^{-5}$	$3.2 \cdot 10^{-2}$	$3 \cdot 10^{-3}$	8.26	0.39
tu [pb]	$9.8 \cdot 10^{-7}$	$1.4 \cdot 10^{-7}$	$2.8 \cdot 10^{-8}$	$2.7 \cdot 10^{-9}$	$1.4 \cdot 10^{-2}$	$1.3 \cdot 10^{-3}$	$6.2 \cdot 10^{-2}$	$2.9 \cdot 10^{-3}$
$t\bar{t}$ [pb]							241.4	15.4

Table 4.5 Benchmark points for different $\mathscr{Z}_N \times \mathscr{Z}_M$ flavour symmetries for inclusive flavon production channels with high flavon mass (m_a) in case of the soft symmetry-breaking scenario at a 100 TeV hadron collider, assuming $f = 500$ GeV.

The LHC is actively searching for light pseudoscalar particles. For a light flavon, present sensitivities of the LHC are given in table 4.6. Using these sensitivities given in table 4.6, the estimated sensitivities for the HL-LHC, HE-LHC, and a 100 TeV collider are given in table 4.7. The benchmark predictions for the processes given in table 4.6, for different $\mathscr{Z}_N \times \mathscr{Z}_M$ flavour symmetries, are given in tables 4.8- 4.10 for $m_a = 20, 60$ GeV for the soft symmetry-breaking scenario.

	$\mathscr{L}[fb^{-1}]$ [References]		ATLAS 13 TeV		CMS 13 TeV	
m_a [GeV]	ATLAS	CMS	20	60	20	60
$\tau\tau$ [pb]		138 [216]				4
$\gamma\gamma$ [pb]	138 [217, 218]	[219]	6	7		

Table 4.6 Current limits of $\sigma \times BR$ at 13 TeV LHC by ATLAS and CMS in low mass resonance searches for inclusive flavon production channels.

	HL-LHC [14 TeV, 3 ab^{-1}]		HE-LHC [27 TeV, 15 ab^{-1}]		100 TeV, 30 ab^{-1}	
m_a [GeV]	20	60	20	60	20	60
$\tau\tau$ [pb]		0.9		0.5		0.6
$\gamma\gamma$ [pb]	1.3	1.5	0.7	0.8	0.8	0.9

Table 4.7 Estimated reach ($\sigma \times BR$) of the HL-LHC, HE-LHC and a 100 TeV collider for low flavon mass (m_a) in inclusive flavon production channels.

We observe from table 4.8 that the HL-LHC provides access only to probe the $\mathscr{Z}_8 \times \mathscr{Z}_{22}$ flavour symmetry through the $\tau\tau$ channel for the mass $m_a = 60$ GeV. The situation changes greatly as we approach the HE-LHC and a 100 TeV hadron collider, as shown in tables 4.9 and 4.10. Now, the $\tau\tau$ channel is accessible for all $\mathscr{Z}_N \times \mathscr{Z}_M$ flavour symmetries. The $\gamma\gamma$ channel and the flavon mass $m_a = 20$ GeV remain beyond the reach of the HL-LHC, HE-LHC and a 100 TeV collider for all flavour symmetries.

	Benchmark $\mathscr{Z}_2 \times \mathscr{Z}_5$		Benchmark $\mathscr{Z}_2 \times \mathscr{Z}_9$		Benchmark $\mathscr{Z}_2 \times \mathscr{Z}_{11}$		Benchmark $\mathscr{Z}_8 \times \mathscr{Z}_{22}$	
m_a [GeV]	20	60	20	60	20	60	20	60
$\tau\tau$ [pb]	$4.7 \cdot 10^{-3}$	0.58	$1.1 \cdot 10^{-2}$	0.62	$2.2 \cdot 10^{-2}$	0.69	$7.7 \cdot 10^{-3}$	9.62
$\gamma\gamma$ [pb]	$5.6 \cdot 10^{-4}$	$1 \cdot 10^{-3}$	$1.5 \cdot 10^{-4}$	$9.9 \cdot 10^{-5}$	$1.1 \cdot 10^{-4}$	$5.8 \cdot 10^{-5}$	$9 \cdot 10^{-5}$	$1.7 \cdot 10^{-2}$

Table 4.8 Benchmark points for different $\mathscr{Z}_N \times \mathscr{Z}_M$ flavour symmetries for inclusive flavon production channels with low flavon mass (m_a) in case of the soft symmetry-breaking scenario at the 14 TeV HL-LHC , assuming $f = 500$ GeV.

	Benchmark $\mathscr{Z}_2 \times \mathscr{Z}_5$		Benchmark $\mathscr{Z}_2 \times \mathscr{Z}_9$		Benchmark $\mathscr{Z}_2 \times \mathscr{Z}_{11}$		Benchmark $\mathscr{Z}_8 \times \mathscr{Z}_{22}$	
m_a [GeV]	20	60	20	60	20	60	20	60
$\tau\tau$ [pb]	$8 \cdot 10^{-3}$	1.06	$2.2 \cdot 10^{-2}$	1.38	$4.2 \cdot 10^{-2}$	1.55	$1.5 \cdot 10^{-2}$	21.78
$\gamma\gamma$ [pb]	$9.4 \cdot 10^{-4}$	$1.8 \cdot 10^{-3}$	$2.9 \cdot 10^{-4}$	$2.2 \cdot 10^{-4}$	$2.2 \cdot 10^{-4}$	$1.3 \cdot 10^{-4}$	$1.7 \cdot 10^{-4}$	$3.8 \cdot 10^{-2}$

Table 4.9 Benchmark points for different $\mathscr{Z}_N \times \mathscr{Z}_M$ flavour symmetries for inclusive flavon production channels with low flavon mass (m_a) in case of the soft symmetry-breaking scenario at the 27 TeV HE-LHC, assuming $f = 500$ GeV.

	Benchmark $\mathscr{Z}_2 \times \mathscr{Z}_5$		Benchmark $\mathscr{Z}_2 \times \mathscr{Z}_9$		Benchmark $\mathscr{Z}_2 \times \mathscr{Z}_{11}$		Benchmark $\mathscr{Z}_8 \times \mathscr{Z}_{22}$	
m_a [GeV]	20	60	20	60	20	60	20	60
$\tau\tau$ [pb]	$2.2 \cdot 10^{-2}$	3.29	$7.5 \cdot 10^{-2}$	5.72	0.15	6.43	$5.1 \cdot 10^{-2}$	92.23
$\gamma\gamma$ [pb]	$2.6 \cdot 10^{-3}$	$5.7 \cdot 10^{-3}$	$9.5 \cdot 10^{-4}$	$9.1 \cdot 10^{-4}$	$7.5 \cdot 10^{-4}$	$5.3 \cdot 10^{-4}$	$5.5 \cdot 10^{-4}$	0.16

Table 4.10 Benchmark points for different $\mathscr{Z}_N \times \mathscr{Z}_M$ flavour symmetries for inclusive flavon production channels with low flavon mass (m_a) in case of the soft symmetry-breaking scenario at a 100 TeV collider, assuming $f = 500$ GeV.

	Benchmark $\mathscr{Z}_2 \times \mathscr{Z}_5$		Benchmark $\mathscr{Z}_2 \times \mathscr{Z}_9$		Benchmark $\mathscr{Z}_2 \times \mathscr{Z}_{11}$	
m_a [GeV]	20	60	20	60	20	60
$\tau\tau$ [pb]	$1.9 \cdot 10^{-7}$	$5.1 \cdot 10^{-4}$	$1.1 \cdot 10^{-11}$	$2 \cdot 10^{-6}$	$2.4 \cdot 10^{-13}$	$3.3 \cdot 10^{-7}$
$\gamma\gamma$ [pb]	$3.8 \cdot 10^{-7}$	$8.8 \cdot 10^{-7}$	$4.5 \cdot 10^{-10}$	$3.2 \cdot 10^{-10}$	$3.8 \cdot 10^{-11}$	$2.7 \cdot 10^{-11}$

Table 4.11 Benchmark points for different $\mathscr{Z}_N \times \mathscr{Z}_M$ flavour symmetries for inclusive flavon production channels with low flavon mass (m_a) in case of the symmetry-conserving scenario at the 14 TeV HL-LHC.

In the symmetry-conserving case, we observe from figures 4.6 and 4.7 that the cross-section can be relatively significant only for a low flavon mass. Therefore, we investigate the symmetry-conserving scenario only for $m_a = 20, 60$ GeV. We show benchmark predictions of symmetry-conserving scenario for different $\mathscr{Z}_{\rm N} \times \mathscr{Z}_{\rm M}$ flavour symmetries in tables 4.11- 4.13 for $m_a = 20, 60$ GeV. It turns out that the inclusive processes in this scenario are beyond the reach of the HL-LHC, HE-LHC, and even a 100 TeV collider.

	Benchmark $\mathscr{Z}_2 \times \mathscr{Z}_5$		Benchmark $\mathscr{Z}_2 \times \mathscr{Z}_9$		Benchmark $\mathscr{Z}_2 \times \mathscr{Z}_{11}$	
m_a [GeV]	20	60	20	60	20	60
$\tau\tau$ [pb]	$2 \cdot 10^{-7}$	$9.2 \cdot 10^{-4}$	$1.8 \cdot 10^{-11}$	$4.5 \cdot 10^{-6}$	$4 \cdot 10^{-13}$	$7.3 \cdot 10^{-7}$
$\gamma\gamma$ [pb]	$6.3 \cdot 10^{-7}$	$1.6 \cdot 10^{-6}$	$8.8 \cdot 10^{-10}$	$7.2 \cdot 10^{-10}$	$7.4 \cdot 10^{-11}$	$6 \cdot 10^{-11}$

Table 4.12 Benchmark points for different $\mathscr{Z}_N \times \mathscr{Z}_M$ flavour symmetries for inclusive flavon production channels with low flavon mass (m_a) in case of the symmetry-conserving scenario at the 27 TeV HE-LHC.

	Benchmark $\mathscr{Z}_2 \times \mathscr{Z}_5$		Benchmark $\mathscr{Z}_2 \times \mathscr{Z}_9$		Benchmark $\mathscr{Z}_2 \times \mathscr{Z}_{11}$	
m_a [GeV]	20	60	20	60	20	60
$\tau\tau$ [pb]	$2.7 \cdot 10^{-10}$	$2.8 \cdot 10^{-3}$	$4.9 \cdot 10^{-11}$	$1.9 \cdot 10^{-5}$	$1.1 \cdot 10^{-12}$	$3 \cdot 10^{-6}$
$\gamma\gamma$ [pb]	$1.7 \cdot 10^{-6}$	$4.9 \cdot 10^{-6}$	$2.8 \cdot 10^{-9}$	$2.9 \cdot 10^{-9}$	$2.4 \cdot 10^{-10}$	$2.5 \cdot 10^{-10}$

Table 4.13 Benchmark points for different $\mathscr{Z}_N \times \mathscr{Z}_M$ flavour symmetries for inclusive flavon production channels with low flavon mass (m_a) in case of the symmetry-conserving scenario at a 100 TeV collider.

4.3.2 Associative production

We notice that there are other channels through which flavon can be produced, as shown in figure 4.10. For instance, the following associated production processes can be used to produce the flavon,

$$bg \to ba,\ ug, cg \to ta, b\bar{b}a \to b\bar{b}\tau^+\tau^-, t\bar{t}a \to t\bar{t}t\bar{t}, \tag{4.8}$$

where the first process undergoes through the flavour-diagonal coupling of the flavon to the $b\bar{b}$, and the second process occurs through the flavour-violating flavon-quark coupling.

The cross-sections of different associative production channels are also shown in figures 4.11 and 4.12. We observe that the production cross sections are, in general, smaller for the soft symmetry-breaking as well as symmetry-conserving scenarios, and can be relatively large only for low flavon mass.

The process $t\bar{t}a \to t\bar{t}t\bar{t}$ can occur only for the $\mathscr{Z}_8 \times \mathscr{Z}_{22}$ flavour symmetry where the flavour-diagonal coupling of the flavon to top quarks is allowed. This results

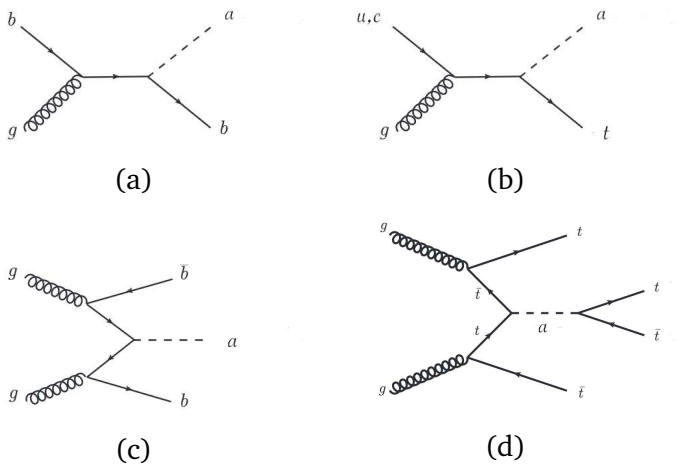

Fig. 4.10 Feynman diagrams for the production of the flavon through different associative channels.

in a relatively large cross-section involving $t\bar{t}$ channels. Thus, the $\mathscr{Z}_8 \times \mathscr{Z}_{22}$ flavour symmetry is very special in this sense.

As noticed in the case of inclusive production of the heavy flavon mass, we observe from figures 4.13 and 4.14 that the associative production cross-sections of the flavon of different $\mathscr{Z}_N \times \mathscr{Z}_M$ flavour symmetries for the VEV $f = 500$ GeV for the soft symmetry-breaking scenario can be sufficiently large. Therefore, we continue to use this choice even for the associative production of the heavy flavon of different $\mathscr{Z}_N \times \mathscr{Z}_M$ flavour symmetries.

	$\mathscr{L}[fb^{-1}]$ [References]		ATLAS 13 TeV		CMS 13 TeV	
m_a [GeV]	ATLAS	CMS	500	1000	500	1000
$t\bar{t}a \to t\bar{t}t\bar{t}$ [pb]	139 [220]	137 [221]	$1 \cdot 10^{-2}$	$6 \cdot 10^{-3}$	$2 \cdot 10^{-2}$	
$gg \to ab\bar{b} \to \tau\tau b\bar{b}$ [pb]	36.1 [205]	35.9 [206]	$8 \cdot 10^{-2}$	$9 \cdot 10^{-3}$	$6 \cdot 10^{-2}$	$1 \cdot 10^{-2}$
$gb \to ab \to \tau\tau b$ [pb])	36.1 [205]	35.9 [206]	$3 \cdot 10^{-2}$	$4 \cdot 10^{-3}$	$3 \cdot 10^{-2}$	$4 \cdot 10^{-3}$

Table 4.14 Current limits of $\sigma \times BR$ at 13 TeV LHC by ATLAS and CMS in resonance searches for associative flavon production channels.

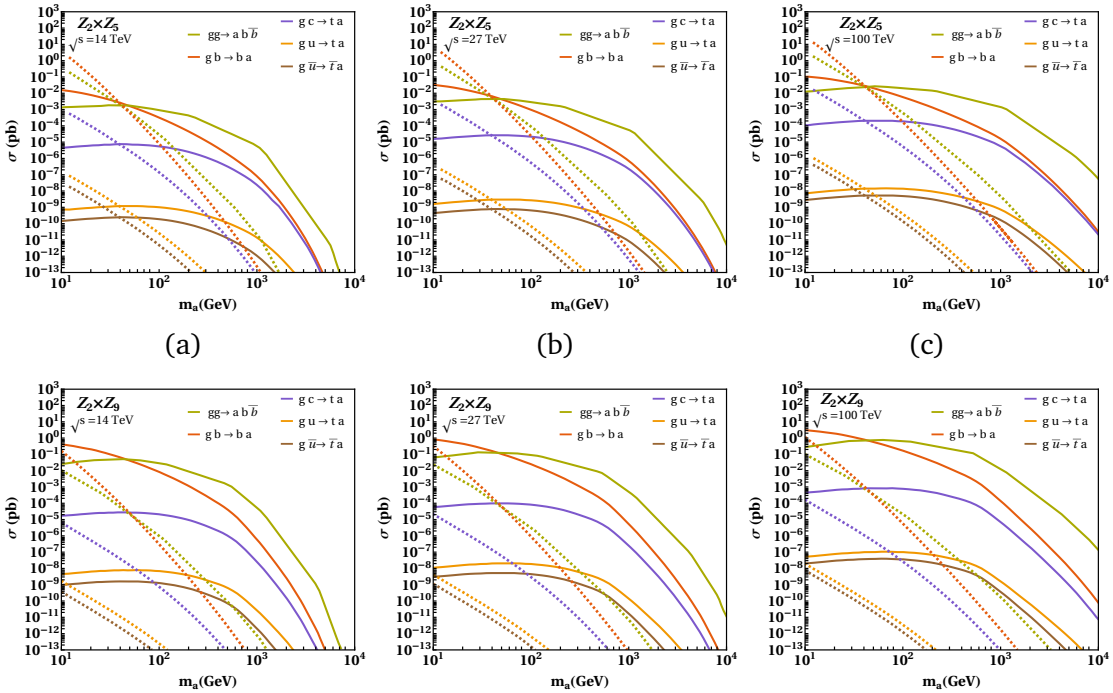

Fig. 4.11 Production cross-sections of the flavon of $\mathscr{Z}_2 \times \mathscr{Z}_5$, and $\mathscr{Z}_2 \times \mathscr{Z}_9$ flavour symmetries with respect to its mass through different channels for 14 TeV HL-LHC, 27 TeV HE-LHC and future 100 TeV collider. The solid lines represents the production cross section along the boundaries of parameter space allowed by the observable $R_{\mu\mu}$ for soft symmetry-breaking scenario, while the dashed lines correspond to that in the symmetry-conserving scenario along the allowed parameter space by the observable $BR(K_L \to \mu\mu)_{SD}$.

The present reach of the LHC for the associative production channels is shown in table 4.14. We show the sensitivities of these modes at the HL-LHC, HE-LHC, and a 100 TeV collider in table 4.15. The primary reason the 100 TeV collider sensitivities appear comparatively poor is the large SM background for a 100 TeV collider, where it turns out that $\sigma_B^{100TeV} \leq 10\sigma_B^{LHC}$. Our benchmark predictions for different $\mathscr{Z}_\mathrm{N} \times \mathscr{Z}_\mathrm{M}$ flavour symmetries, are given in tables 4.16- 4.18 for the soft symmetry-breaking scenario.

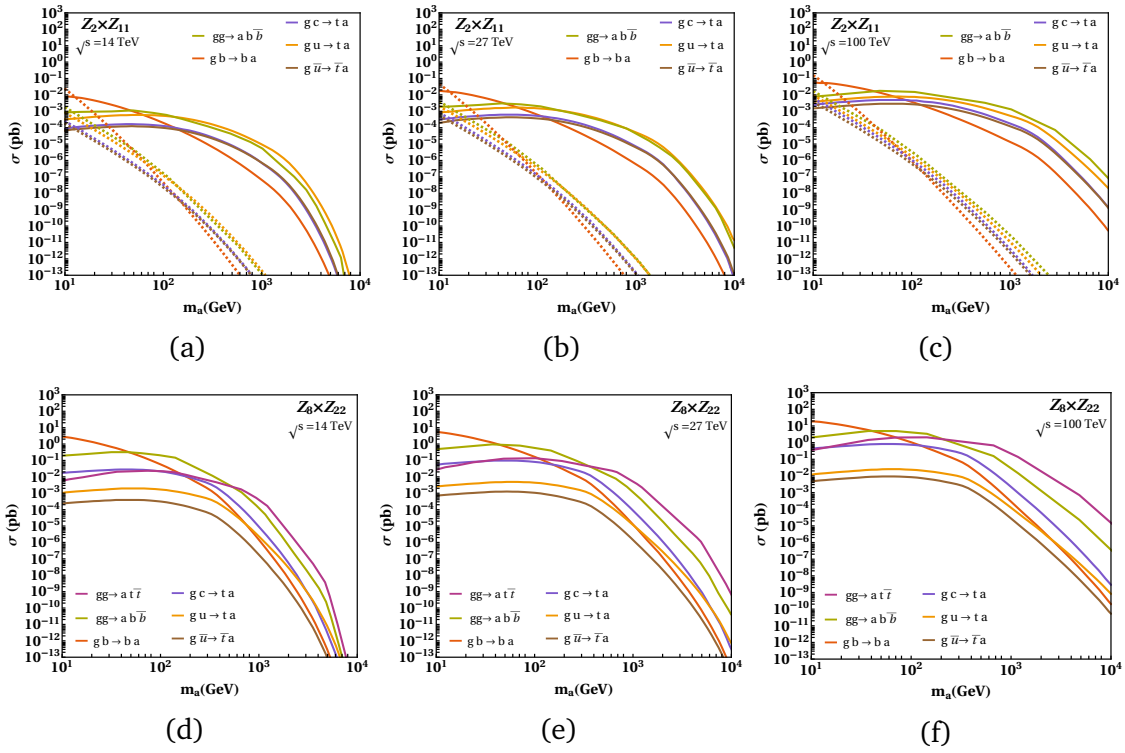

Fig. 4.12 Production cross-sections of the flavon of $\mathscr{Z}_2 \times \mathscr{Z}_{11}$, and $\mathscr{Z}_8 \times \mathscr{Z}_{22}$ flavour symmetries with respect to its mass through different channels for 14 TeV HL-LHC, 27 TeV HE-LHC and future 100 TeV collider. The solid lines represents the production cross section along the boundaries of parameter space allowed by the observable $R_{\mu\mu}$ for soft symmetry-breaking scenario, while the dashed lines correspond to that in the symmetry-conserving scenario along the allowed parameter space by the observable $BR(K_L \to \mu\mu)_{SD}$.

	HL-LHC [14 TeV, 3 ab^{-1}]		HE-LHC [27 TeV, 15 ab^{-1}]		100 TeV, 30 ab^{-1}	
m_a [GeV]	500	1000	500	1000	500	1000
$t\bar{t}a \to t\bar{t}t\bar{t}$ [pb]	$2 \cdot 10^{-3}$	$1 \cdot 10^{-3}$	$3 \cdot 10^{-3}$	$2 \cdot 10^{-3}$	$1 \cdot 10^{-2}$	$9 \cdot 10^{-3}$
$gg \to ab\bar{b} \to \tau\tau b\bar{b}$ [pb]	$7 \cdot 10^{-3}$	$1 \cdot 10^{-3}$	$5 \cdot 10^{-3}$	$8 \cdot 10^{-4}$	$8 \cdot 10^{-3}$	$1 \cdot 10^{-3}$
$gb \to ab \to \tau\tau b$ [pb]	$3 \cdot 10^{-3}$	$5 \cdot 10^{-4}$	$2 \cdot 10^{-3}$	$3 \cdot 10^{-4}$	$4 \cdot 10^{-3}$	$5 \cdot 10^{-4}$

Table 4.15 Estimated reach ($\sigma \times BR$) of HL-LHC, HE-LHC and the 100 TeV collider for high flavon mass (m_a) in associative flavon production channels.

We observe from table 4.16 that only the mode $t\bar{t}a \to t\bar{t}t\bar{t}$ is within the reach of the HL-LHC for the flavon mass $m_a = 500$ GeV for the $\mathscr{Z}_8 \times \mathscr{Z}_{22}$ flavour symmetry.

This scenario improves slightly at the HE-LHC and at a 100 TeV collider for the $\mathscr{Z}_8 \times \mathscr{Z}_{22}$ flavour symmetry such that the flavon mass $m_a = 1000$ GeV becomes also accessible. The symmetry-conserving scenario remains beyond the reach of the HL-LHC, HE-LHC and a 100 TeV collider for the associative production modes. Therefore, we do not discuss it anymore in this case.

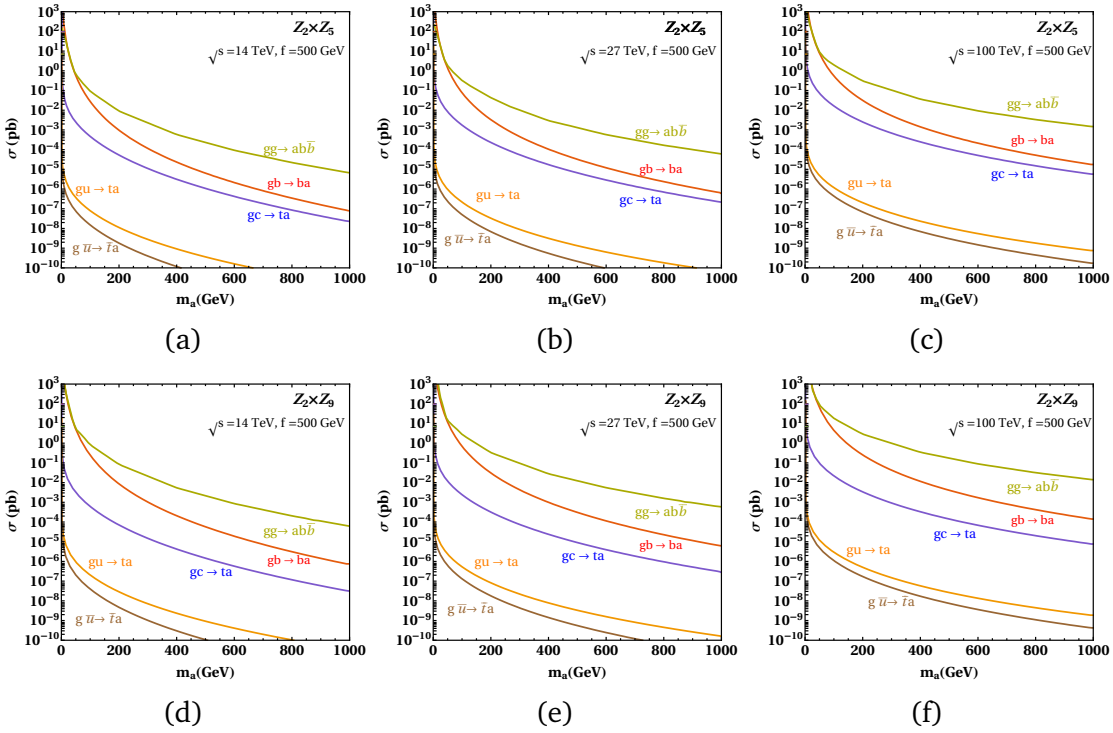

Fig. 4.13 Production cross-sections of the flavon of $\mathscr{Z}_2 \times \mathscr{Z}_5$, and $\mathscr{Z}_2 \times \mathscr{Z}_9$ flavour symmetries with respect to its mass through different channels for 14 TeV HL-LHC, 27 TeV HE-LHC, and future 100 TeV hadron collider, where the flavon VEV $f = 500$ GeV.

	Benchmark $\mathscr{Z}_2 \times \mathscr{Z}_5$		Benchmark $\mathscr{Z}_2 \times \mathscr{Z}_9$		Benchmark $\mathscr{Z}_2 \times \mathscr{Z}_{11}$		Benchmark $\mathscr{Z}_8 \times \mathscr{Z}_{22}$	
m_a [GeV]	500	1000	500	1000	500	1000	500	1000
$t\bar{t}a \to t\bar{t}t\bar{t}$ [pb]							$\boxed{1.6 \cdot 10^{-3}}$	$1.6 \cdot 10^{-4}$
$gg \to ab\bar{b} \to \tau\tau b\bar{b}$ [pb]	$6 \cdot 10^{-7}$	$1.8 \cdot 10^{-8}$	$1 \cdot 10^{-4}$	$3.2 \cdot 10^{-6}$	$3.4 \cdot 10^{-5}$	$8.9 \cdot 10^{-7}$	$1.6 \cdot 10^{-6}$	$3.2 \cdot 10^{-8}$
$gb \to ab \to \tau\tau b$ [pb]	$1.7 \cdot 10^{-7}$	$5.6 \cdot 10^{-9}$	$2.9 \cdot 10^{-5}$	$9.7 \cdot 10^{-7}$	$9.4 \cdot 10^{-6}$	$2.7 \cdot 10^{-7}$	$4.5 \cdot 10^{-7}$	$9.7 \cdot 10^{-9}$

Table 4.16 Benchmark points for different $\mathscr{Z}_N \times \mathscr{Z}_M$ flavour symmetries for associative flavon production channels with high flavon mass (m_a) in case of the soft symmetry-breaking at the 14 TeV HL-LHC, assuming $f = 500$ GeV.

	Benchmark $\mathscr{Z}_2 \times \mathscr{Z}_5$		Benchmark $\mathscr{Z}_2 \times \mathscr{Z}_9$		Benchmark $\mathscr{Z}_2 \times \mathscr{Z}_{11}$		Benchmark $\mathscr{Z}_8 \times \mathscr{Z}_{22}$	
m_a [GeV]	500	1000	500	1000	500	1000	500	1000
$t\bar{t}a \to t\bar{t}t\bar{t}$ [pb]							$\boxed{1.5 \cdot 10^{-2}}$	$\boxed{2.3 \cdot 10^{-3}}$
$gg \to ab\bar{b} \to \tau\tau b\bar{b}$ [pb]	$3.3 \cdot 10^{-6}$	$1.6 \cdot 10^{-7}$	$5.8 \cdot 10^{-4}$	$2.8 \cdot 10^{-5}$	$1.9 \cdot 10^{-4}$	$7.9 \cdot 10^{-6}$	$9 \cdot 10^{-6}$	$2.8 \cdot 10^{-7}$
$gb \to ab \to \tau\tau b$ [pb]	$9.3 \cdot 10^{-7}$	$5.1 \cdot 10^{-8}$	$1.6 \cdot 10^{-4}$	$8.8 \cdot 10^{-6}$	$5.3 \cdot 10^{-5}$	$2.5 \cdot 10^{-6}$	$2.5 \cdot 10^{-6}$	$8.8 \cdot 10^{-8}$

Table 4.17 Benchmark points for different $\mathscr{Z}_N \times \mathscr{Z}_M$ flavour symmetries for associative flavon production channels with high flavon mass (m_a) in case of the soft symmetry-breaking at the 27 TeV HE-LHC, assuming $f = 500$ GeV.

	Benchmark $\mathscr{Z}_2 \times \mathscr{Z}_5$		Benchmark $\mathscr{Z}_2 \times \mathscr{Z}_9$		Benchmark $\mathscr{Z}_2 \times \mathscr{Z}_{11}$		Benchmark $\mathscr{Z}_8 \times \mathscr{Z}_{22}$	
m_a [GeV]	500	1000	500	1000	500	1000	500	1000
$t\bar{t}a \to t\bar{t}t\bar{t}$ [pb]							$\boxed{0.41}$	$\boxed{9.6 \cdot 10^{-2}}$
$gg \to ab\bar{b} \to \tau\tau b\bar{b}$ [pb]	$4.7 \cdot 10^{-5}$	$4.0 \cdot 10^{-6}$	$8.2 \cdot 10^{-3}$	$6.9 \cdot 10^{-4}$	$2.7 \cdot 10^{-3}$	$1.9 \cdot 10^{-4}$	$1.3 \cdot 10^{-4}$	$6.8 \cdot 10^{-6}$
$gb \to ab \to \tau\tau b$ [pb]	$1.34 \cdot 10^{-5}$	$1.23 \cdot 10^{-6}$	$2.3 \cdot 10^{-3}$	$2.1 \cdot 10^{-4}$	$7.5 \cdot 10^{-4}$	$6.0 \cdot 10^{-5}$	$3.6 \cdot 10^{-5}$	$2.1 \cdot 10^{-6}$

Table 4.18 Benchmark points for different $\mathscr{Z}_N \times \mathscr{Z}_M$ flavour symmetries for associative flavon production channels with high flavon mass (m_a) in case of the soft symmetry-breaking scenario at a 100 TeV collider, assuming $f = 500$ GeV.

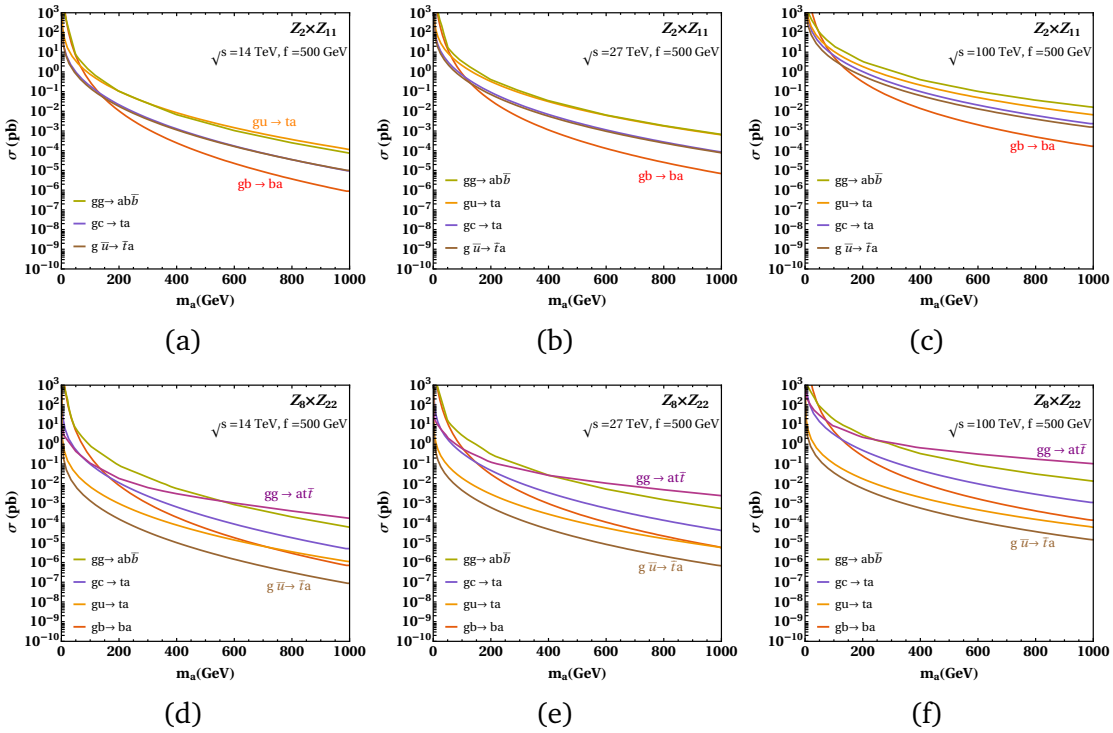

Fig. 4.14 Production cross-sections of the flavon of $\mathscr{Z}_2 \times \mathscr{Z}_{11}$, and $\mathscr{Z}_8 \times \mathscr{Z}_{22}$ flavour symmetries with respect to its mass through different channels for 14 TeV HL-LHC, 27 TeV HE-LHC, and future 100 TeV hadron collider, where the flavon VEV $f = 500$ GeV.

4.3.3 Di-flavon production

In this section, we discuss the production of di-flavon, which is an important mode to explore the flavon physics of different $\mathscr{Z}_N \times \mathscr{Z}_M$ flavour symmetries. We show the present LHC sensitivities of di-flavon channels in table 4.19. The reach of the HL-LHC, HE-LHC and a 100 TeV collider is given in table 4.20. The di-flavon production cross-sections for different $\mathscr{Z}_N \times \mathscr{Z}_M$ flavour symmetries are shown in figure 4.15 in the case of soft symmetry-breaking scenario.

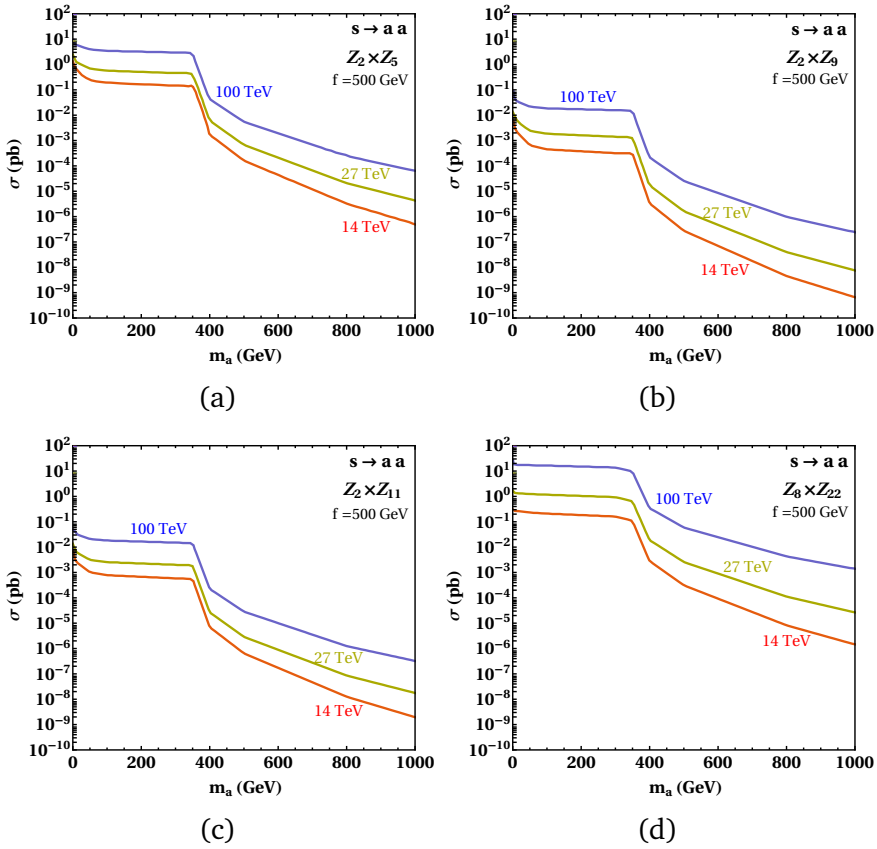

Fig. 4.15 Production cross-sections of the di-flavon in $\mathscr{Z}_2 \times \mathscr{Z}_5$, $\mathscr{Z}_2 \times \mathscr{Z}_9$, $\mathscr{Z}_2 \times \mathscr{Z}_{11}$, and $\mathscr{Z}_8 \times \mathscr{Z}_{22}$ flavour symmetries with respect to its mass for 14 TeV HL-LHC, 27 TeV HE-LHC, and 100 TeV hadron collider, where the flavon VEV $f = 500$ GeV.

The benchmark predictions for different $\mathscr{Z}_N \times \mathscr{Z}_M$ flavour symmetries, are given in tables 4.21- 4.23 for the soft symmetry-breaking scenario and heavy flavon masses. We observe from tables 4.21- 4.23 that the di-flavon production for heavy flavon mass is insensitive to the HL-LHC, HE-LHC and even to a 100 TeV collider for all $\mathscr{Z}_N \times \mathscr{Z}_M$ flavour symmetries.

	$\mathscr{L}[fb^{-1}]$ [References]		ATLAS 13 TeV		CMS 13 TeV	
m_a [GeV]	ATLAS	CMS	500	1000	500	1000
$s \to aa \to b\bar{b}\ell\ell$ [pb]	36.1 [222]	19.7 [223][a]	$2 \cdot 10^{-2}$	$1 \cdot 10^{-2}$	$2 \cdot 10^{-1}$	$2 \cdot 10^{-2}$
$s \to aa \to b\bar{b}b\bar{b}$ [pb]	36.1 [224]	35.9 [225]	$4 \cdot 10^{-2}$	$9 \cdot 10^{-3}$	$7 \cdot 10^{-2}$	$1 \cdot 10^{-2}$

[a]The reference [223] is at sqrt(s) = 8 TeV.

Table 4.19 Current limits of $\sigma \times BR$ at 13 TeV LHC by ATLAS and CMS in high mass resonance searches for di-flavon production channels.

	HL-LHC [14 TeV, 3 ab^{-1}]		HE-LHC [27 TeV, 15 ab^{-1}]		100 TeV, 30 ab^{-1}	
m_a [GeV]	500	1000	500	1000	500	1000
$s \to aa \to b\bar{b}\tau\tau$ [pb]	$2 \cdot 10^{-3}$	$1 \cdot 10^{-3}$	$2 \cdot 10^{-3}$	$8 \cdot 10^{-4}$	$3 \cdot 10^{-3}$	$1 \cdot 10^{-3}$
$s \to aa \to b\bar{b}b\bar{b}$ [pb]	$5 \cdot 10^{-3}$	$1 \cdot 10^{-3}$	$3 \cdot 10^{-3}$	$7 \cdot 10^{-4}$	$5 \cdot 10^{-3}$	$1 \cdot 10^{-3}$

Table 4.20 Estimated reach ($\sigma \times BR$) of HL-LHC, HE-LHC and the 100 TeV collider for high flavon mass (m_a) in di-flavon production channels.

	Benchmark $\mathscr{Z}_2 \times \mathscr{Z}_5$		Benchmark $\mathscr{Z}_2 \times \mathscr{Z}_9$		Benchmark $\mathscr{Z}_2 \times \mathscr{Z}_{11}$		Benchmark $\mathscr{Z}_8 \times \mathscr{Z}_{22}$	
m_a [GeV]	500	1000	500	1000	500	1000	500	1000
$s \to aa \to b\bar{b}\tau\tau$ [pb]	$1.4 \cdot 10^{-8}$	$4.4 \cdot 10^{-11}$	$7 \cdot 10^{-9}$	$1.7 \cdot 10^{-11}$	$7.5 \cdot 10^{-10}$	$1.7 \cdot 10^{-12}$	$2 \cdot 10^{-9}$	$3.7 \cdot 10^{-12}$
$s \to aa \to b\bar{b}\mu\mu$ [pb]	$1.3 \cdot 10^{-11}$	$4 \cdot 10^{-14}$	$1.5 \cdot 10^{-10}$	$3.6 \cdot 10^{-13}$	$5.8 \cdot 10^{-12}$	$1.3 \cdot 10^{-14}$	$1.8 \cdot 10^{-11}$	$3.2 \cdot 10^{-14}$
$s \to aa \to b\bar{b}b\bar{b}$ [pb]	$4 \cdot 10^{-8}$	$1.3 \cdot 10^{-10}$	$1.8 \cdot 10^{-8}$	$4.3 \cdot 10^{-11}$	$1.1 \cdot 10^{-9}$	$2.6 \cdot 10^{-12}$	$4.9 \cdot 10^{-9}$	$9.1 \cdot 10^{-12}$

Table 4.21 Benchmark points for different $\mathscr{Z}_N \times \mathscr{Z}_M$ flavour symmetries for di-flavon production channels with high flavon mass (m_a) in case of the soft symmetry-breaking scenario at the 14 TeV HL-LHC, assuming $f = 500$ GeV.

	Benchmark $\mathscr{Z}_2 \times \mathscr{Z}_5$		Benchmark $\mathscr{Z}_2 \times \mathscr{Z}_9$		Benchmark $\mathscr{Z}_2 \times \mathscr{Z}_{11}$		Benchmark $\mathscr{Z}_8 \times \mathscr{Z}_{22}$	
m_a [GeV]	500	1000	500	1000	500	1000	500	1000
$s \to aa \to b\bar{b}\tau\tau$ [pb]	$5.9 \cdot 10^{-8}$	$3.7 \cdot 10^{-10}$	$4.2 \cdot 10^{-8}$	$1.9 \cdot 10^{-10}$	$3.4 \cdot 10^{-9}$	$1.5 \cdot 10^{-11}$	$1.6 \cdot 10^{-8}$	$6.9 \cdot 10^{-11}$
$s \to aa \to b\bar{b}\mu\mu$ [pb]	$5.3 \cdot 10^{-11}$	$3.4 \cdot 10^{-13}$	$9.1 \cdot 10^{-10}$	$4.2 \cdot 10^{-12}$	$2.6 \cdot 10^{-11}$	$1.2 \cdot 10^{-13}$	$1.4 \cdot 10^{-10}$	$5.9 \cdot 10^{-13}$
$s \to aa \to b\bar{b}b\bar{b}$ [pb]	$1.7 \cdot 10^{-7}$	$1.1 \cdot 10^{-9}$	$1.1 \cdot 10^{-7}$	$4.9 \cdot 10^{-10}$	$5.1 \cdot 10^{-9}$	$2.3 \cdot 10^{-11}$	$4 \cdot 10^{-8}$	$1.7 \cdot 10^{-10}$

Table 4.22 Benchmark points for different $\mathscr{Z}_N \times \mathscr{Z}_M$ flavour symmetries for di-flavon production channels with high flavon mass (m_a) in case of the soft symmetry-breaking scenario at the 27 TeV HE-LHC, assuming $f = 500$ GeV.

	Benchmark $\mathscr{Z}_2 \times \mathscr{Z}_5$		Benchmark $\mathscr{Z}_2 \times \mathscr{Z}_9$		Benchmark $\mathscr{Z}_2 \times \mathscr{Z}_{11}$		Benchmark $\mathscr{Z}_8 \times \mathscr{Z}_{22}$	
m_a [GeV]	500	1000	500	1000	500	1000	500	1000
$s \to aa \to b\bar{b}\tau\tau$ [pb]	$4.8 \cdot 10^{-7}$	$5.5 \cdot 10^{-9}$	$6.5 \cdot 10^{-7}$	$6.2 \cdot 10^{-9}$	$3.3 \cdot 10^{-8}$	$2.8 \cdot 10^{-10}$	$3.7 \cdot 10^{-7}$	$3.5 \cdot 10^{-9}$
$s \to aa \to b\bar{b}\mu\mu$ [pb]	$4.2 \cdot 10^{-10}$	$4.9 \cdot 10^{-12}$	$1.4 \cdot 10^{-8}$	$1.3 \cdot 10^{-10}$	$2.5 \cdot 10^{-10}$	$2.2 \cdot 10^{-12}$	$3.2 \cdot 10^{-9}$	$3.1 \cdot 10^{-11}$
$s \to aa \to b\bar{b}b\bar{b}$ [pb]	$1.4 \cdot 10^{-6}$	$1.6 \cdot 10^{-8}$	$1.7 \cdot 10^{-6}$	$1.6 \cdot 10^{-8}$	$5 \cdot 10^{-8}$	$4.3 \cdot 10^{-10}$	$9.1 \cdot 10^{-7}$	$8.6 \cdot 10^{-9}$

Table 4.23 Benchmark points for different $\mathscr{Z}_N \times \mathscr{Z}_M$ flavour symmetries for di-flavon production channels with high flavon mass (m_a) in case of the soft symmetry-breaking scenario at a 100 TeV collider, assuming $f = 500$ GeV.

We observed earlier that the di-flavon production of a heavy mass flavon is beyond the reach of HL-LHC, HE-LHC, and a 100 TeV collider for different $\mathscr{Z}_{\rm N} \times \mathscr{Z}_{\rm M}$ flavour symmetries. However, this scenario changes in the case of a light flavon. We show the present sensitivities of the light di-flavon searches of the LHC in table 4.24. The sensitivities of the HL-LHC, HE-LHC, and a 100 TeV collider for a light di-flavon productions are shown in table 4.25.

	$\mathscr{L}[fb^{-1}]$ [References]		ATLAS 13 TeV		CMS 13 TeV	
m_a [GeV]	ATLAS	CMS	20	60	20	60
$s \to aa \to b\bar{b}\ell\ell$ [pb]	139 [226]	138 [227]	$1 \cdot 10^{-4}$	$1 \cdot 10^{-4}$	$9 \cdot 10^{-5}$	$8 \cdot 10^{-5}$
$s \to aa \to b\bar{b}b\bar{b}$ [pb]	36.1 [228]	138 [229]	3	1	1	$3 \cdot 10^{-1}$

Table 4.24 Current limits of $\sigma \times BR$ at 13 TeV LHC by ATLAS and CMS in low mass resonance searches for di-flavon channels.

	HL-LHC [14 TeV, 3 ab^{-1}]		HE-LHC [27 TeV, 15 ab^{-1}]		100 TeV, 30 ab^{-1}	
m_a [GeV]	20	60	20	60	20	60
$s \to aa \to b\bar{b}\ell\ell$ [pb]	$2 \cdot 10^{-5}$	$2 \cdot 10^{-5}$	$1 \cdot 10^{-5}$	$1 \cdot 10^{-5}$	$2 \cdot 10^{-5}$	$2 \cdot 10^{-5}$
$s \to aa \to b\bar{b}b\bar{b}$ [pb]	0.2	$7 \cdot 10^{-2}$	0.16	$5 \cdot 10^{-2}$	0.2	$7 \cdot 10^{-2}$

Table 4.25 Estimated reach ($\sigma \times BR$) of HL-LHC, HE-LHC and the 100 TeV collider for low flavon mass (m_a) in di-flavon production channels.

We show our benchmark predictions of di-flavon production cross-sections in tables 4.26-4.28 for low flavon masses in the soft symmetry-breaking scenario. We observe that $aa \to b\bar{b}\tau\tau$ mode is accessible for all $\mathscr{Z}_{\rm N} \times \mathscr{Z}_{\rm M}$ flavour symmetries at the HL-LHC, HE-LHC, and a 100 TeV collider. All three channels are sensitive to the HL-LHC, HE-LHC, and a 100 TeV collider only for the $\mathscr{Z}_8 \times \mathscr{Z}_{22}$ flavour symmetry. The production cross-sections in the symmetry-conserving scenario are too small to be under the reach of any collider, as observed in tables 4.29-4.31.

	Benchmark $\mathscr{Z}_2 \times \mathscr{Z}_5$		Benchmark $\mathscr{Z}_2 \times \mathscr{Z}_9$		Benchmark $\mathscr{Z}_2 \times \mathscr{Z}_{11}$		Benchmark $\mathscr{Z}_8 \times \mathscr{Z}_{22}$	
m_a [GeV]	20	60	20	60	20	60	20	60
$s \to aa \to b\bar{b}\tau\tau$ [pb]	$2.7 \cdot 10^{-5}$	$1.9 \cdot 10^{-5}$	$3.2 \cdot 10^{-5}$	$1.5 \cdot 10^{-5}$	$3.3 \cdot 10^{-5}$	$2 \cdot 10^{-5}$	$1.8 \cdot 10^{-2}$	$1.6 \cdot 10^{-2}$
$s \to aa \to b\bar{b}\mu\mu$ [pb]	$2.5 \cdot 10^{-8}$	$1.7 \cdot 10^{-8}$	$7.2 \cdot 10^{-7}$	$3.3 \cdot 10^{-7}$	$2.7 \cdot 10^{-7}$	$1.5 \cdot 10^{-7}$	$1.6 \cdot 10^{-4}$	$1.3 \cdot 10^{-4}$
$s \to aa \to b\bar{b}b\bar{b}$ [pb]	$6.8 \cdot 10^{-5}$	$5.4 \cdot 10^{-5}$	$6.1 \cdot 10^{-5}$	$3.7 \cdot 10^{-5}$	$4.1 \cdot 10^{-5}$	$2.9 \cdot 10^{-5}$	$3.6 \cdot 10^{-2}$	$3.7 \cdot 10^{-2}$

Table 4.26 Benchmark points for different $\mathscr{Z}_N \times \mathscr{Z}_M$ flavour symmetries for diflavon production channels with low flavon mass (m_a) in case of the soft symmetry-breaking scenario at the 14 TeV HL-LHC, assuming $f = 500$ GeV.

	Benchmark $\mathscr{Z}_2 \times \mathscr{Z}_5$		Benchmark $\mathscr{Z}_2 \times \mathscr{Z}_9$		Benchmark $\mathscr{Z}_2 \times \mathscr{Z}_{11}$		Benchmark $\mathscr{Z}_8 \times \mathscr{Z}_{22}$	
m_a [GeV]	20	60	20	60	20	60	20	60
$s \to aa \to b\bar{b}\tau\tau$ [pb]	$6.8 \cdot 10^{-5}$	$5.5 \cdot 10^{-5}$	$9.5 \cdot 10^{-5}$	$5.8 \cdot 10^{-5}$	$8.9 \cdot 10^{-5}$	$6.1 \cdot 10^{-5}$	$8.8 \cdot 10^{-2}$	$8.1 \cdot 10^{-2}$
$s \to aa \to b\bar{b}\mu\mu$ [pb]	$6.4 \cdot 10^{-8}$	$5 \cdot 10^{-8}$	$2.2 \cdot 10^{-6}$	$1.3 \cdot 10^{-6}$	$7.1 \cdot 10^{-7}$	$4.7 \cdot 10^{-7}$	$8 \cdot 10^{-4}$	$7 \cdot 10^{-4}$
$s \to aa \to b\bar{b}b\bar{b}$ [pb]	$1.7 \cdot 10^{-4}$	$1.6 \cdot 10^{-4}$	$1.8 \cdot 10^{-4}$	$1.4 \cdot 10^{-4}$	$1.1 \cdot 10^{-4}$	$9.2 \cdot 10^{-5}$	0.18	0.19

Table 4.27 Benchmark points for different $\mathscr{Z}_N \times \mathscr{Z}_M$ flavour symmetries for diflavon production channels with low flavon mass (m_a) in case of the soft symmetry-breaking scenario at the 27 TeV HE-LHC, assuming $f = 500$ GeV.

	Benchmark $\mathscr{Z}_2 \times \mathscr{Z}_5$		Benchmark $\mathscr{Z}_2 \times \mathscr{Z}_9$		Benchmark $\mathscr{Z}_2 \times \mathscr{Z}_{11}$		Benchmark $\mathscr{Z}_8 \times \mathscr{Z}_{22}$	
m_a [GeV]	20	60	20	60	20	60	20	60
$s \to aa \to b\bar{b}\tau\tau$ [pb]	$3.5 \cdot 10^{-4}$	$3.2 \cdot 10^{-4}$	$6.9 \cdot 10^{-4}$	$5.5 \cdot 10^{-4}$	$5.2 \cdot 10^{-4}$	$4.2 \cdot 10^{-4}$	1.17	1.11
$s \to aa \to b\bar{b}\mu\mu$ [pb]	$3.3 \cdot 10^{-7}$	$2.9 \cdot 10^{-7}$	$1.6 \cdot 10^{-5}$	$1.2 \cdot 10^{-5}$	$4.2 \cdot 10^{-6}$	$3.2 \cdot 10^{-6}$	$1.1 \cdot 10^{-2}$	$9.7 \cdot 10^{-3}$
$s \to aa \to b\bar{b}b\bar{b}$ [pb]	$8.8 \cdot 10^{-4}$	$9.2 \cdot 10^{-4}$	$1.3 \cdot 10^{-3}$	$1.3 \cdot 10^{-3}$	$6.4 \cdot 10^{-4}$	$6.3 \cdot 10^{-4}$	2.35	2.65

Table 4.28 Benchmark points for different $\mathscr{Z}_N \times \mathscr{Z}_M$ flavour symmetries for diflavon production channels with low flavon mass (m_a) in case of the soft symmetry-breaking scenario at a 100 TeV collider, assuming $f = 500$ GeV.

	Benchmark $\mathscr{Z}_2 \times \mathscr{Z}_5$		Benchmark $\mathscr{Z}_2 \times \mathscr{Z}_9$		Benchmark $\mathscr{Z}_2 \times \mathscr{Z}_{11}$	
m_a [GeV]	20	60	20	60	20	60
$s \to aa \to b\bar{b}\tau\tau$ [pb]	$8.7 \cdot 10^{-10}$	$3.5 \cdot 10^{-12}$	$1.9 \cdot 10^{-14}$	$5.4 \cdot 10^{-17}$	$3.4 \cdot 10^{-16}$	$1.1 \cdot 10^{-18}$
$s \to aa \to b\bar{b}\mu\mu$ [pb]	$8.2 \cdot 10^{-13}$	$3.2 \cdot 10^{-15}$	$4.2 \cdot 10^{-16}$	$1.2 \cdot 10^{-18}$	$2.7 \cdot 10^{-18}$	$8.8 \cdot 10^{-21}$
$s \to aa \to b\bar{b}b\bar{b}$ [pb]	$2.2 \cdot 10^{-9}$	$1 \cdot 10^{-11}$	$3.6 \cdot 10^{-14}$	$1.3 \cdot 10^{-16}$	$4.2 \cdot 10^{-16}$	$1.7 \cdot 10^{-18}$

Table 4.29 Benchmark points for different $\mathscr{Z}_N \times \mathscr{Z}_M$ flavour symmetries for di-flavon production channels with low flavon mass (m_a) in case of the symmetry-conserving scenario at the 14 TeV HL-LHC.

	Benchmark $\mathscr{Z}_2 \times \mathscr{Z}_5$		Benchmark $\mathscr{Z}_2 \times \mathscr{Z}_9$		Benchmark $\mathscr{Z}_2 \times \mathscr{Z}_{11}$	
m_a [GeV]	20	60	20	60	20	60
$s \to aa \to b\bar{b}\tau\tau$ [pb]	$1.9 \cdot 10^{-9}$	$8.8 \cdot 10^{-12}$	$4.7 \cdot 10^{-14}$	$1.6 \cdot 10^{-16}$	$7.7 \cdot 10^{-16}$	$3 \cdot 10^{-18}$
$s \to aa \to b\bar{b}\mu\mu$ [pb]	$1.8 \cdot 10^{-12}$	$7.9 \cdot 10^{-15}$	$1.1 \cdot 10^{-15}$	$3.6 \cdot 10^{-18}$	$6.2 \cdot 10^{-18}$	$2.3 \cdot 10^{-20}$
$s \to aa \to b\bar{b}b\bar{b}$ [pb]	$4.7 \cdot 10^{-9}$	$2.5 \cdot 10^{-11}$	$9.1 \cdot 10^{-14}$	$4.1 \cdot 10^{-16}$	$9.5 \cdot 10^{-16}$	$3.1 \cdot 10^{-18}$

Table 4.30 Benchmark points for different $\mathscr{Z}_N \times \mathscr{Z}_M$ flavour symmetries for di-flavon production channels with low flavon mass (m_a) in case of the symmetry-conserving scenario at the 27 TeV HE-LHC.

	Benchmark $\mathscr{Z}_2 \times \mathscr{Z}_5$		Benchmark $\mathscr{Z}_2 \times \mathscr{Z}_9$		Benchmark $\mathscr{Z}_2 \times \mathscr{Z}_{11}$	
m_a [GeV]	20	60	20	60	20	60
$s \to aa \to b\bar{b}\tau\tau$ [pb]	$7.8 \cdot 10^{-9}$	$4.5 \cdot 10^{-11}$	$2.4 \cdot 10^{-13}$	$1.2 \cdot 10^{-15}$	$3.4 \cdot 10^{-15}$	$1.7 \cdot 10^{-17}$
$s \to aa \to b\bar{b}\mu\mu$ [pb]	$7.4 \cdot 10^{-12}$	$4 \cdot 10^{-14}$	$5.5 \cdot 10^{-15}$	$2.5 \cdot 10^{-17}$	$2.8 \cdot 10^{-17}$	$1.3 \cdot 10^{-19}$
$s \to aa \to b\bar{b}b\bar{b}$ [pb]	$2 \cdot 10^{-8}$	$1.3 \cdot 10^{-10}$	$4.7 \cdot 10^{-13}$	$2.8 \cdot 10^{-15}$	$4.2 \cdot 10^{-15}$	$2.6 \cdot 10^{-17}$

Table 4.31 Benchmark points for different $\mathscr{Z}_N \times \mathscr{Z}_M$ flavour symmetries for di-flavon production channels with low flavon mass (m_a) in case of the symmetry-conserving scenario at a 100 TeV collider.